Chapter 1

Reversible Deactivation Radical Polymerization: State-of-the-Art in 2017

Sivaprakash Shanmugam and Krzysztof Matyjaszewski*

Center for Macromolecular Engineering, Department of Chemistry, Carnegie Mellon University, 4400 Fifth Avenue, Pittsburgh, Pennsylvania 15213, United States
***E-mail: matyjaszewski@cmu.edu.**

This chapter highlights the current advancements in reversible-deactivation radical polymerization (RDRP) with a specific focus on atom transfer radical polymerization (ATRP). The chapter begins with highlighting the termination pathways for acrylates radicals that were recently explored via RDRP techniques. This led to a better understanding of the catalytic radical termination (CRT) in ATRP for acrylate radicals. The designed new ligands for ATRP also enabled the suppression of CRT and increased chain end functionality. In addition, further mechanistic understandings of SARA-ATRP with Cu^0 activation and comproportionation were studied using model reactions with different ligands and alkyl halide initiators. Another focus of RDRP in recent years has been on systems that are regulated by external stimuli such as light, electricity, mechanical forces and chemical redox reactions. Recent advancements made in RDRP in the field of complex polymeric architectures, organic-inorganic hybrid materials and bioconjugates have also been summarized.

Introduction

The overarching goal of this chapter is to provide an overall summary of the recent achievements in reversible-deactivation radical polymerization (RDRP), primarily in atom transfer radical polymerization (ATRP), and also in reversible addition-fragmentation chain transfer (RAFT) polymerization, tellurium mediated

Matyjaszewski et al.; Reversible Deactivation Radical Polymerization: Mechanisms and Synthetic Methodologies
ACS Symposium Series; American Chemical Society: Washington, DC, 2018.

polymerization (TERP), iodine mediated polymerization (IMP), and nitroxide mediated polymerization (NMP). Of these techniques, progress in ATRP will be covered in more depth, since subsequent chapters in this book will provide more insights into the development of the other RDRP techniques especially RAFT polymerization. Due to the large volume of literature generated over the years, the discussion on the progress of these techniques will be focused on recent literature spanning from 2013 to 2017, since the last ACS Meeting on Controlled Radical Polymerization (*1*, *2*). Nevertheless, readers are directed to several excellent reviews for in-depth discussions on the different areas explored (*3*–*7*). Initial sections will explore the recent discoveries in catalytic radical termination (CRT) in ATRP, design of a novel ligand that reduces CRT, and insights into ATRP in the presence of Cu^0. In addition, as polymer chemists aim to design complex macromolecules similar to protein and DNA found in nature, achieving spatial, temporal, sequence and stereochemical regulations during polymer synthesis has recently become the central theme of RDRP. This book chapter will highlight the recent literature on photochemical, electrochemical, and mechanochemical means of achieving these goals. These achievements in externally regulated polymer synthesis are translated into advancing the synthesis of complex polymeric architectures, hybrid materials (polymer brushes), and bioconjugates. The advancements in these areas will also be highlighted.

Advancements in ATRP

Mechanism of Catalytic Radical Termination (CRT) in ATRP

In the discussion of novel mechanisms and initiation pathways, it is paramount to highlight the fundamental importance of understanding the mechanism of radical termination. Dispersity, which is a measure of polymer molecular weight distribution, relies on monomer conversion, number of monomer addition per activation/deactivation cycle, and amount of dead chains. As current literature often neglects the termination factor in calculation of dispersity for ATRP, a new dispersity expression by blending dormant and dead chain populations was recently derived (*8*). Bimolecular radical termination relies on two pathways – disproportionation and combination. In disproportionation, two chains, one with saturated chain end and the with unsaturated chain end, are formed. In combination, a single chain is made through C-C coupling (*9*). The pathway of chain termination in radical polymerization relies on the nature of the radical species involved. Styrene and acrylonitrile propagating radicals undergo chain termination primarily through combination while methacrylate radicals terminate by both disproportionation and combination (*10*). Different methods to study selectivity of radical termination have been proposed but these methods were unable to provide definitive conclusions. For instance, the ratios of disproportionation to combination for polymerizations of methyl methacrylate (MMA) and styrene (St) vary between reports despite identical polymerization conditions (*11*). A new method to study radical termination with TERP was proposed. The use of TERP allowed for activation of organotellurium dormant species by photoirradiation to generate polymer-end radical. This method was

used to estimate ratio of disproportionation to combination for poly(methyl methacrylate) and polystyrene radicals that approximately agreed with previous reports (*11*). In comparison to the well understood termination of PSt and PMMA radicals, termination of acrylate radicals was a subject of intense debate. A recent report claimed that acrylate radicals generated from organotellurium polymerizations are terminated primarily (99%) through disproportionation at room temperature (*12*). *Ab initio* molecular dynamics computations suggested that the polyacrylate radicals can be terminated through a direct disproportionation reaction as well as a new stepwise process involving initial formation of C-O coupling product followed by intramolecular rearrangement. In a subsequent study, an avenue to control the ratio of disproportionation to combination for termination of MMA and St radicals using TERP was suggested by changing reaction temperature and viscosity (*13*). Disproportionation was proposed to be favored over combination at lower temperature and higher viscosity. The observed viscosity effect in the selection of mode of termination was reasoned with an "advanced collision model", a derivative of the collision model proposed by Fischer (*14*). The proposed model suggested that combination was more viscosity sensitive than disproportionation, and therefore, an increase in viscosity should result in a more significant retardation of the rate constant for combination than of that observed for disproportionation (*13*). However, a subsequent investigation revealed that alkyl radicals generated through the decomposition of diazo initiator dimethyl 2,2′-azobis(isobutyrate) (V-601), which directly generate methacrylate radicals, yielded similar Disp/Comb ratios in a large range of temperatures and viscosities (*15*). The discrepancies with the previously discussed results were explained by the role of alkyl tellurium radical acting as a catalyst for disproportionation. In a typical V-601 promoted termination, bimolecular chain coupling took place within the solvent cage or outside the solvent cage. In the case of TERP mediated polymerization, cage escape was needed to enable bimolecular termination as possible side reaction that involved β-H abstraction from the carbon-based radical by tellanyl radicals took place within the solvent cage. They formed alkene and Te-H species which generated saturated chain ends in a fast reaction with macroradicals.

Metals such as iron have been successfully implemented in both organometallic-mediated radical polymerization (OMRP) and ATRP (*16–18*), but copper complexes which are widely used in ATRP have not been adapted for OMRP despite the proven existence of copper (II) organometallic complexes (*19*). Nevertheless, attempts have been made to characterize these organometallic intermediates. For instance, EPR measurements were carried out to characterize copper (II) species generated in CRT. By following the reaction of $[Cu^{I}]^{+}$ formed in the presence of poly(butyl acrylate) radicals by EPR, a new signal distinct from $[Cu^{II}(TPMA)Br]^{+}$ complex was observed (*20*). Organometallic complexes generated in ATRP were also investigated by electrochemical reduction and UV-Vis. These findings revealed that radicals generated from bromoacetonitrile and chloroacetonitrile (to a lesser extent ethyl α-bromoisobutyrate), react with $[Cu^{I}(TPMA)]^{+}$ and $[Cu^{I}(Me_6tren)]^{+}$ in dimethylsulfoxide (DMSO) and acetonitrile (ACN) to form cupric complexes with alkyl moiety in the axial coordination site (*19*).

As ATRP systems contain highly active copper catalysts, additional side reactions where acrylate radicals can react with L/Cu^{I} to reversibly generate a complex (L/Cu^{II}-polyacrylate. These species can then undergo catalytic radical termination (CRT) which is proposed as the primary mode of termination of acrylate radicals in ATRP (*21*). The CRT process often results in termination of acrylates to form disproportionation-like products in a tris(2-pyridylmethyl)amine (TPMA)-copper catalyzed ATRP (*22*). Thus, a study to better understand the bimolecular termination and CRT in ATRP was designed. Poly(methyl acrylate) terminated with bromine end group was activated with copper(I) complexes with tris[2-(dimethylamino)ethyl]amine (Me_6TREN), tris(2-pyridylmethyl)amine (TPMA) or tris-(3,5-dimethyl-4-methoxy-2-pyridylmethyl)amine (TPMA*[3]) in the absence of monomer (*23*). Under conditions kinetically promoting bimolecular termination, size exclusion chromatography (SEC) revealed a polymer product with double molecular weight relative to macroinitiator distribution indicating a termination pathway via radical combination. Likewise, conditions kinetically promoting CRT resulted in no shifting in macroinitiator distribution in SEC, suggesting products resembling disproportionation of polymer chains. PREDICI simulations for TPMA mediated termination reactions highlighted the importance of midchain radical generated from acrylate radical backbiting in the termination profile. Majority of the terminated chains originated from CRT and cross-termination between secondary and tertiary midchain radicals (Scheme 1). Further studies into the mechanistic pathways of acrylate termination will be discussed in another chapter.

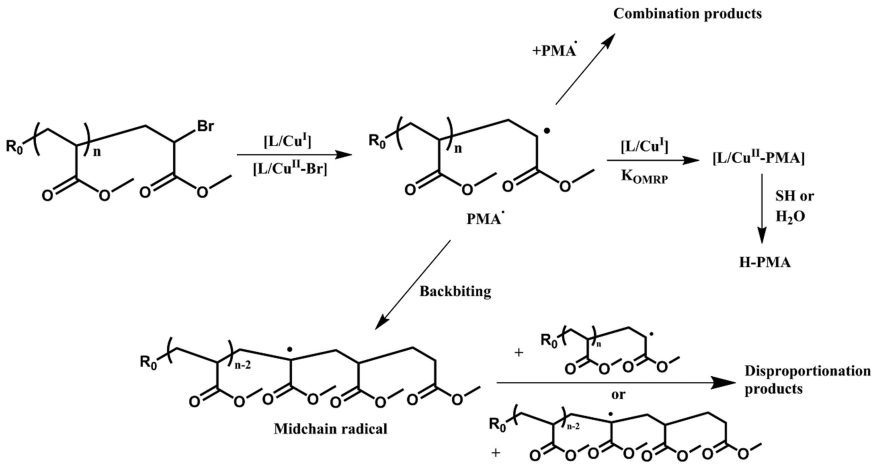

Scheme 1. Proposed mechanistic pathways for acrylate radical termination in ATRP.

Design of New Ligands for ATRP

The recent exploitation of reducing agents in ATRP significantly decreased the amount of copper complexes needed for polymerization (*24*). In order to

further reduce the amount of copper complexes in polymerizations, significant efforts were placed towards development of more active catalysts by fine tuning the ligand structure to tailor electronic properties of copper(I) center. To achieve this goal, electron-donating groups were systematically incorporated to highly active ATRP ligands to further increase the reactivity copper(I) complex. For instance, a series of novel Cu (I and II) complexes with TPMA-based ligands containing 4-methoxy-3,5-dimethylsubstituted pyridine arms were reported (*25*). Cyclic voltammetry measurements revealed that by increasing substitution of electron donating groups in the 4 (-OMe) and 3,5 (-Me) positions of the pyridine rings in TPMA, the reactivity of the copper(I) complexes also increases due to increased stabilization of copper(II) oxidation state (*25*). In addition, design of new ligands allowed for better understanding of the CRT process. Polymerization of n-butyl acrylate (BA) with azobis(isobutyronitrile) (AIBN) in the presence of copper complexes with tridentate and tetradentate ligands showed higher rates of CRT for more reducing copper complexes with higher ATRP activity. On the other hand, ligand denticity had smaller effect on polymerization kinetics but affected the rate determining step for CRT (*26*). Recently, tris[(4-dimethylaminiopyridyl) methyl]amine ($TPMA^{NMe2}$) was reported as a novel ligand for ATRP. The $TPMA^{NMe2}$ based copper catalyst was ~1 billion times more active than seminal bipyridine-based catalyst, ~300 000 more active than TPMA, and ~30 000 more active than Me_6TREN. Polymerization of acrylates via ICAR and Ag^0 ATRP were well-controlled for catalyst loadings as low as 10 ppm relative to monomer. The high values of activation rate constants of ATRP and low concentration of $TPMA_{NMe2}/Cu^I$ suppressed CRT and allowed for high-end functionality (*27*).

Progress in SARA-ATRP

Traditional ATRP systems often required the use of large amounts of copper catalyst (>1000 ppm) to account for the conversion of Cu^I activator to Cu^{II} deactivator due to termination reactions. However, by slow and continuous reduction process, controlled polymerizations can be carried out using as low as <10 ppm of copper complex. The build-up of Cu^{II} deactivator due to unavoidable termination reactions can be reduced back to Cu^I activator. One example of reducing agent that can be added is Cu^0 which can acts as both a supplemental activator (SA) of alkyl halides and reducing agent (RA) for Cu^{II}, and therefore, aptly terming the process as SARA-ATRP (*28–31*). A recent Cu^0 mediated polymerization provided a set of universal conditions to perform polymerization for acrylates, methacrylates and styrene using commercially available and inexpensive reagents, such as PMDETA (*N*,*N*′,*N*′′,*N*′′′,*N*′′′-pentamethyldiethylenetriamine), isopropanol and Cu^0 wire (*32*). Isopropanol is not a good solvent for some of the resulting polymers and Cu complexes and a surprising accelerated kinetics at higher temperatures could be associated with solubility changes of activators and deactivators at variable temperatures. Although Cu^0 is able to activate alkyl halide, majority activation (99%) still takes place from highly active Cu^I catalysts (*29*, *30*, *33*, *34*). In addition, comproportionation between Cu^0 and Cu^{II} to generate Cu^I is the dominant process in comparison to disproportionation of Cu^I in polar

organic solvents such as DMSO and also kinetically dominant even in water (*29*, *35–37*). In a recent attempt, Cu^0 activation and comproportionation was studied using model reactions with three different ligands, including Me_6TREN, TPMA, and PMDETA, in the presence of three different alkyl halides, including methyl 2-bromopropionate (MBrP), ethyl α-bromoisobutyrate (EBiB), and ethyl α-bromophenylacetate (EBPA) using solvents such as ACN, dimethylformamide (DMF) and DMSO (*38*). Cu^I/ligand with lower reduction potential linearly increased ATRP activation rate coefficient (k_a) in solution (*25*, *39*). A similar effect was seen in activation with less active ligands and alkyl halides by Cu^0. The chemical step involving atom transfer reaction was the rate determining step, however, the surface activation with more active ligand reached the same value for all active substrates. This is a typical behavior of heterogeneous reactions where adsorption/desorption instead of chemical reaction become the rate determining step. The activation rate achieved did not surpass the comproportionation rate hinting that both reactions could have the same rate determining step, the desorption of Cu^I from the surface of Cu^0. This study was expanded to understand the mechanism of alkyl halide activation at the surface by carrying out model reactions with less active MBrP with activation rate limited by surface atom transfer assisted by ligand, and very active EBPA with activation rate limited by desorption and adsorption of Cu^I from surfaces, using Me_6TREN ligand in the DMSO and acetonitrile (*40*). At low reactant concentrations, first order reaction was observed for both alkyl halide initiator and ligand, while high reactant concentrations led to zero order reaction for both ligand and initiator. The absence of ligand led to poor activation of EBPA with no activation for MBrP while increasing the amount of ligand above certain concentration did not increase the activation rate as it competed with alkyl halides for access to the Cu^0 surface. The surface area of Cu^0 activation rate of the EBPA and MBrP followed the first order kinetics where adsorption of these initiators onto Cu^0 surface facilitated carbon-bromine bond cleavage through the inner sphere electron transfer (ISET) mechanism.

Photochemical, Electrochemical, and Mechanochemical Regulation in RDRP

Photochemical ATRP

An important progress in RDRP has been achieved in polymer synthesis mediated by external stimuli including applied current (*41–55*). Light (*56–58*), mechanical force (*59–62*), and chemical redox triggers (*63–66*) to enable spatial, temporal, and sequence control. Several reviews are available on these different external stimuli techniques and interested readers are directed to these works (*6*, *57*, *58*, *67–73*). This section highlights several external regulations in ATRP via photochemical, electrochemical, and sonochemical means during the last few years. This section also covers recent progress in photochemical IMP and TERP. As external regulation for RAFT polymerization is covered in the following chapters, it will not be highlighted here.

Photomediated ATRP under visible LED lights (violet and blue) and sunlight was initially performed in the presence of copper catalyst using ATRP initiators, EBiB for acrylates and ethyl α-bromophenylacetate (EBPA) for methacrylates, and TPMA, PMDETA, and tris((4-methoxy-3,5-dimethylpyridin-2-yl)-methyl) amine ligands (*74–77*). This approach enabled temporal control over polymerization where polymerization was promoted in the presence of light and suppressed in the absence of light. Initial polymerizations of MMA and MA were carried out in DMF while polymerization of oligo(ethylene glycol) methyl ether methacrylate (OEGMA) was promoted in water with TPMA using 100 ppm of $CuBr_2$. Further optimizations for aqueous polymerization of OEGMA/TPMA/ $CuBr_2$ system led to reduction of copper loadings to as low as 20 ppm in the presence of sodium bromide (*78*). Based on experimental and kinetic modelling, photo-ATRP was proposed to take place through an ARGET-ATRP pathway where Cu^{II} complexes were reduced by free amine ligands to generate Cu^{I} activator species and initiating radicals (Scheme 2A) (*79*, *80*). The oxidized amine radical cation could then initiate new chains after proton transfer. Although interaction between alkyl halide and amine ligand can generate radicals via photochemical ICAR-ATRP, this was a minor pathway as it was one order magnitude slower than reduction of Cu^{II} by electron donor through photo-ATRP.

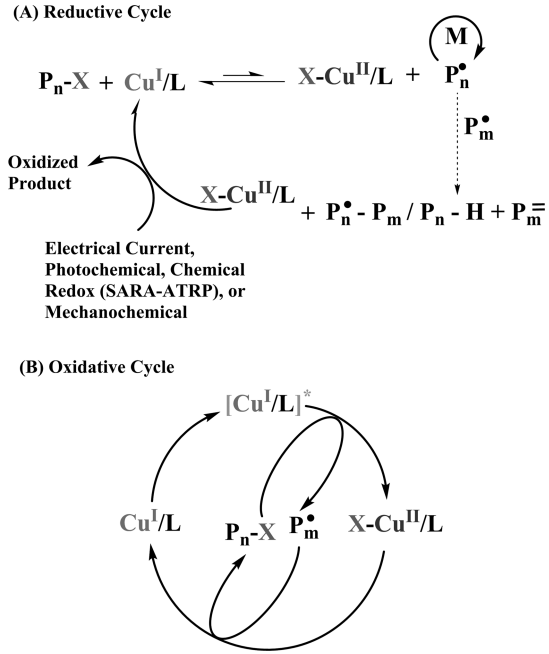

Scheme 2. Proposed mechanism for copper mediated polymerization under reductive quenching cycle (A) activated by electricity, light, sonication or redox chemistry, and oxidative quenching cycle (B) activated by visible-light irradiation.

In another investigation, UV-mediated photo-ATRP was also performed with excess aliphatic tertiary amine, Me_6TREN, to initiate polymerization of acrylates, methacrylates and styrene (*81*). Polymerization under UV irradiation in DMSO led to high monomer conversions (92-97%) with low dispersities with a ratio of [$CuBr_2$]:[Me_6TREN] of 1:6 (*81*, *82*). A survey of various solvents including ionic liquids (*40*, *41*) and water (*83*) for polymerization of a wide range of hydrophilic, hydrophobic and functional monomers was performed to demonstrate the versatility of $CuBr_2$/Me_6TREN catalytic system (*84*). In addition, the range of photocatalysts used to mediate polymerization was also expanded to copper(II) formate-Me_6TREN (*85*, *86*) and copper gluconate (*85*, *87*). The photo-ATRP was studied using pulsed-laser polymerization (PLP) and electrospray-ionization mass spectrometry (ESI-MS) for better mechanistic understandings (*88*). The main pathway of initiation depended on the reaction of alkyl bromide to CuBr/L. The ligand played an important as a reducing agent of $CuBr_2$. The high extinction coefficient of $CuBr_2$/Me_6TREN allowed the complex to enter the excited state before being quenched by another Me_6TREN to generate CuBr/Me_6TREN and cation radical Me_6TREN in the dominant pathway.

In addition to using tertiary amine as reductive quenchers for photo-ATRP, oxidative quenching pathways for activation of polymerization were also explored (Scheme 2B). Thus, bis(1,10-phenanthroline)copper(I) ($Cu(phen)_2^+$) was excited under visible light to enable reduction of EBPA initiator for polymerization MMA which resulted in the formation propagating radical and $CuBr_2$ (*89*, *90*). The copper (I) complex was regenerated upon deactivation of $CuBr_2$ by a propagating radical. Parallel to the reduction cycle for copper mediated photo-ATRP described above, polymerization only took place in the presence of irradiation and was completely suppressed in the absence of light. Similar oxidative cycles were also implemented for photo-ATRP of acrylates and methacrylates using transition metal photocatalysts such as *fac*-$Ir(ppy)_3$ (*91–95*) and iron halides (*96–103*). For instance, iron mediated photo-ATRP for polymerization of methacrylates was demonstrated without the need for additional ligands, reducing agents, and radical initiators (*96*). Polar solvent such as DMF and ACN directly solubilized iron(III) bromide ($FeBr_3$) without ligands. Polymerization of different methacrylates, including MMA, ethyl methacrylate (EMA), benzyl methacrylate (BzMA), *n*-butyl methacrylate (*n*BMA), trimethylsilyloxyethyl methacrylate (TMSEMA), and furfuryl methacrylate (FMA) (*96*, *104*), resulted in well-defined homopolymers and block copolymers. Photolysis of $FeBr_3$ generated $FeBr_2$ and bromine radical under UV light with the latter reacting with MMA to form 2,3-dibromoisobutyrate initiator. The *in situ* generation of initiator under UV light enabled the polymerization to proceed without the need for external addition of initiator.

Metal-Free ATRP (o-ATRP)

In an effort to reduce residual metal in ATRP, a recent focus has been centered on expanding metal free catalysis to promote polymerization under visible light (*105*). The first example of metal free ATRP was introduced by Miyake where excited state perylene reduced alkyl bromide to promote polymerization of

methacrylates and styrene under visible light and sunlight irradiation (*106*). This work was further expanded to include pyrene and anthracene to mediate metal free photo-ATRP (*107*). Although these polynuclear hydrocarbons imposed spatio-temporal control over polymerization, similar to photo-ATRP with copper, iridium and iron complexes, these organic catalysts showed low initiation efficiency with alkyl halides leading to limited control over molecular weight of the synthesized polymer. Further improvements to metal-free ATRP was through the implementation of 10-phenylphenothiazine (PTH) catalyst and variations to this catalyst for polymerization of methacrylates (*105*) and acrylonitrile (*108*). Moreover, the absorption of PTH primarily in the UV region was expanded into the visible region, around 400 nm, with phenyl benzo[*b*]phenothiazine (*109*). Optimization of organocatalysis for ATRP via computational modelling led to a novel class of photocatalysts with 5,10-diphenyl-5,10-dihydrophenazine core that could activate alkyl halide initiators via electron transfer under photoirradiation. Photocatalysts with dihydrophenazine and *N*-aryl phenoxazine cores with various electron donating, neutral and electron withdrawing functionalities were designed based on computational modelling and tested experimentally to determine their efficiency in promoting polymerization (*110–114*). Mechanistic investigations revealed that phenoxazines and dihydrophenazines have a faster activation and deactivation rate in comparison to phenothiazines as they maintain their planar state with little reorganization in the triplet and radical cation states (*115*). Nevertheless, a different activation mechanism was suggested based on investigation of transient vibrational and electronic absorption spectroscopy with sub-picosecond time resolution: electron transfer from short-lived singlet excited state gave better control of molecular weight and dispersity by suppressing the formation of excess radicals (*75*). Furthermore, visible light photocatalysts such as xanthene dyes in the presence of reducing amines such as fluorescein/trimethylamine (*116*), and fluorescein, Eosin Y (EY), and erythrosine B (EB) with PMDETA (*117*) were also explored for polymerization of different acrylates and methacrylates with photo-ATRP.

Electrochemical and Mechanochemical ATRP

The current advances in electrochemistry and mechanochemistry in ATRP and in organic synthesis were reviewed (*118–120*). A unique advantage of electrochemistry is that it can reduce activators to deactivators but also efficiently oxidized activators to deactivators and halt polymerization. It can also electrodeposit Cu on the electrode and recycle transition metals. *e*ATRP solved an important challenge in ATRP pertaining to polymerization of acidic monomers (i.e. intramolecular cyclization reaction that leads to the loss of carbon-halogen chain end functionality). Electrochemical ATRP (eATRP) was successfully implemented in the synthesis of poly(methacrylic acid) (PMAA) by promoting a fast polymerization with chlorine atom as the chain-end halogen under acidic conditions (Scheme 3) (*121*). In addition, a fundamental understanding on the mechanism of aqueous ATRP was possible through electrochemistry which provided a guideline for performing ATRP in water (*122*).

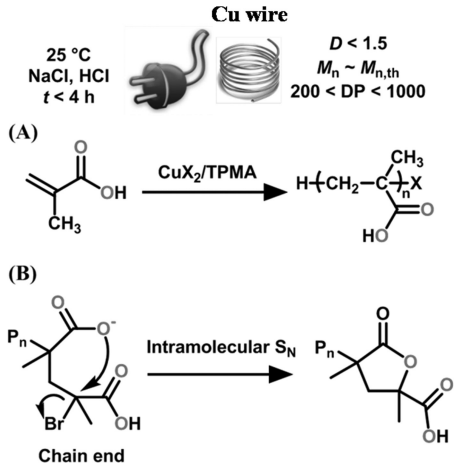

Scheme 3. Promoting fast polymerization of MAA in water with chlorine initiator (A) via eATRP while suppressing intramolecular cyclization observed with bromo initiator (B). Reproduced with permission from ref. (121). Copyright 2016, American Chemical Society.

The use of piezoelectric barium titanate ($BaTiO_3$) nanoparticles under ultrasonic agitation was successfully implemented for water splitting (potential -1.23 V) (*123*). The highly reducing nature of the nanoparticle was further exploited to reduce Cu(II) catalyst mechanochemically under ultrasonic agitation in the presence of barium titanate nanoparticles to generate Cu(I) which with EBiB initiated ATRP of BA monomer to yield polymers with low dispersities (*124*). Initial work with $BaTiO_3$ required the use of high catalyst loadings (10 000 ppm with respect to monomer) leading to low molecular weight PBA (M_n < 3000). Further expansion of mechano-ATRP was carried out with ultrasound in the presence of low concentration copper catalysts (75 ppm, Cu/TPMA), which enabled the synthesis of well-defined PMA (Scheme 4) (*125*). In this investigation, various shapes (cubic or tetragonal) and sizes (50-100 nm) of $BaTiO_3$ nanoparticles under different catalytic loadings were tested to optimize the reaction conditions. As barium titanate tend to aggregate and precipitate in solution without ultrasound, it was stabilized through surface modification with PMMA which enhanced the rate of polymerization. The concept of mechano-induced electron transfer was further expanded to included zinc oxide piezoelectric nanoparticles to enable well-defined polymerization of acrylates and methacrylates (*126*).

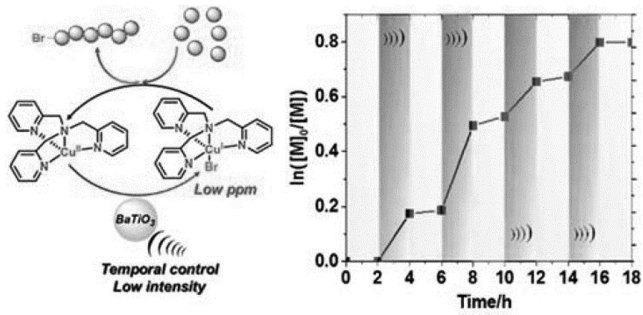

Scheme 4. Sonochemical ATRP mediated by piezoelectric barium titanate ($BaTiO_3$) nanoparticles by interfacial reduction of Cu^{II}/TPMA complex leading to the formation of activator for ATRP. Reproduced with permission from ref. (125). Copyright 2017, American Chemical Society.

Photochemical TERP and IMP

Photomediated TERP with initiating radicals generated from a dormant organotellurium species by C-Te photolysis was reported (*127*). This report was followed up by optimization of conditions for TERP polymerization under low light intensity and mild temperature conditions with overall control of the progress of polymerization (*128*). In depth understanding on the photophysical properties of organotellurium compounds were later explored (*2*, *129*). As tellurium compounds have a broad absorption range with maximum absorption at 350 nm, this led to the n(Te)-σ*(C-Te) transition upon irradiation and generated radicals that initiated polymerization in the presence of monomer. The high quantum yield of the C-Te bond homolysis led to initiation even under low light intensity. As the process can be carried out under low temperature, back-biting reaction in acrylate polymerization was essentially avoided. Benzoyl phenyltelluride was later introduced as a highly reactive TERP reagent capable of initiating under visible light irradiation (400-500 nm) for well-defined polymerization of acrylates and acrylamides (*130*).

In the iodine transfer polymerization, a catalyst-free iodine mediated polymerization was initiated under abroad range of visible wavelengths (460-720 nm) (*131*, *132*). In solvents such as dimethylacetamide (DMAc), DMSO and DMF, homolysis of carbon-iodine bond was promoted through coordination with solvent molecules under irradiation. The generation of carbon radicals through this method enabled the polymerization of methacrylates through a reversible termination instead of degenerate chain transfer mechanism. Photoinduced reversible complexation mediated polymerization (photo-RCMP) was later developed allowing for photolysis of a dormant alkyl iodide in the presence of tributylamine (TBA), enabling polymerization of methacrylates (*133*). This system was then expanded to functional monomers with glycidol, ethylene glycol or amino functional groups, such as 2-(dimethylamino)ethyl methacrylate (DMAEMA), POEGMA and glycidyl methacrylate (GMA), for

direct complexation with 2-cyanopropyl iodide (CPI) photoinitiator that led to polymerization under blue light irradiation (*134*). Photo-RCMP also utilized tertiary anilines as photo-organocatalysts that absorb in a wide range of visible light wavelengths (*135*). These photocatalysts acted as energy antennas for photon absorption with the light energy then transfer to alkyl iodide resulting in photolysis of carbon-iodide bond. The generated radicals were successfully used for polymerization of methacrylates.

Advancements in Polymers with Complex Architecture

Ultra-High Molecular Weight Polymers

RDRP techniques have enabled excellent control over the molecular weights of different functional monomers, and therefore, providing an avenue for synthesis of hyperbranched (*136*, *137*), star (*138*, *139*), brush (*140*, *141*), and block copolymers (*71*, *142–144*), while also providing narrow and tunable (*145*, *146*) molecular weight distributions. Nevertheless, achieving ultra-high molecular weights (UHMW) in the range of 8 x 10^6 has only been possible under high pressure (*147–149*) and heterogeneous conditions (*150*, *151*). A novel approach to achieve UHMW polymers was explored with polymerization *N,N*-dimethylacrylamide (DMA) in water using trithiocarbonate, 2-(2-carboxyethylsulfanylthiocarbonylsulfanyl)-2-methylpropionic acid, which acted as a photoiniferter under UV irradiation (365 nm) (*152*). The high propagation rate constant of DMA in water and the reversible termination with photoiniferter at high solution viscosity due to UHMW of polymer chains were key features permitting control. At UHMW, decrease in translational diffusion was reduced due to high viscosity preventing radical termination. This approach resulted in PDMA chains with MW excess of 8 million. UHMW synthesis was also achieved under oxygen tolerant condition using enzyme-cascade catalysis using pyranose oxidase (P2Ox) and horseradish peroxidase (HRP) where oxygen molecules were initially reduced in the presence of glucose by P2Ox to generate hydrogen peroxide (*153*). The hydrogen peroxide was then used by HRP in the presence of acetyl acetonate (ACAC) to generate radicals that initiated RAFT polymerization. Polymerization of DMA conducted with this approach resulted in UHMW polymer with molecular weight of 2×10^6.

Multiblock Copolymers

One of the biggest challenges in chain growth polymerization techniques is sequence control over addition of monomers units. Several techniques have been developed for synthesis of multiblock copolymers with the aim of synthesizing near-quantitative conversion for each block, avoiding purification steps, and enabling narrow molecular weight distributions with high end-group functionality (*154–157*). Introduction of multiblock sequence controlled polymerization with RAFT led to the generation of icosablock DMA, 4-acryloylmorpholine (NAM), *N,N*-diethylacrylamide (DEA) and *N*-isopropylacrylamide (NIPAM)

copolymer in aqueous media (*143*, *155*, *158–161*). However, this system became limited due to restriction of monomer selection to acrylamides with polymerization carried out at high temperatures (~70 °C) which may not be suitable for monomers with LCST such as NIPAM. Improving these deficiencies, 'transition metal' and 'sulfur-free' polymerization approach combined with an emulsion biomimetic segregation strategy was envisioned for sequence controlled synthesis of multiblock methacrylate copolymers which can be easily scaled up (*162*). This strategy relied on a vinyl-terminated PMMA macromonomer, synthesized through catalytic chain transfer polymerization (CCTP), that played the role as a chain transfer agent for RAFT polymerization of various methacrylate monomers. CCTP approach with low-spin d_6 Co(II) complexes (cobaloximes) led to abstraction of hydrogen from methacrylic radical to yield Co(III)-H intermediate and a polymer terminated with vinyl group. The generated vinyl-terminated PMMA macromonomers showed chain transfer activity followed by fragmentation to generate macroradical that initiated a second monomer. The compartmentalization provided by emulsion polymerization accelerated polymerization while maintaining slow radical termination. This approach was used for hydrophobic methacrylates such as BMA, BzMA, EHA, and MMA which led to the successful synthesis of heneicosablock (21 blocks) copolymer that exhibited relatively narrow molecular weight distribution. Initial investigations on sulfur free RAFT polymerization, which relied on the use of PMMA macromonomers, was later expanded by synthesizing macromonomers composed of BMA, BzMA, and EHA that led to the successful synthesis of sequence defined multiblock copolymers (*163*).

Multiblock synthesis in ATRP was initially carried out employing Cu(0) which provided acrylic hexablock copolymer in high yields with each block having at least two monomer units added (*154*, *164*, *165*). Upon targeting blocks with higher degree of polymerization, an average of 100 monomer units per block, triblock and quasi-pentablock copolymers was prepared. Nevertheless, this approach becomes limiting as full monomer conversions cannot be achieved (*166*). ATRP in the presence of Cu^0 was later used to generate multiblock glycopolymers with a monomer sequence control (*167*, *168*) as well as multiblock copolymers of acrylamides in less than 5 hours (*169*, *170*). Photo-ATRP enabled a novel route for exploring polymer composition and microstructure at high monomer conversions with good end group fidelity (*93*, *157*, *171–174*). UV mediated ATRP has enabled sequence controlled multiblock copolymers (octablock, hexablock and pentablock copolymers) synthesized in a single pot (*157*). A large number of acrylate monomers were suitable for the synthesis of sequence defined multiblock copolymers including OEGMA, tert-butyl acrylate (tBA), glycidyl acrylate (GA) and solketal acrylate (SA). For instance, under optimized conditions these acrylates have been used to generate undecablock (11 blocks), tridecablock (13 blocks), and tricosablock (23 block) copolymers with narrow molecular distribution with high monomer conversions achieved in each iterative monomer addition steps (*93*, *175*). A faster polymerization was also achieved by synthesizing homopolymers and block copolymers in a short period of time while maintaining high end group fidelity by adapting photo-ATRP into milli-flow and micro-flow reactors (*176*).

Sequence Defined Oligomers

In addition to high molecular weight multiblocks, the development of photo-RAFT enabled the precise synthesis of dimers, trimers, as well as hexamers (combination of two trimers) by using single monomer insertions reactions (*177*). This approach relies on utilizing RAFT agents with high transfer constants, with low propagation rate which ensures addition of only a single monomer unit. The approach was later expanded to include RAFT photoiniferter polymerization with thiolene and esterification reactions to generate discrete pentamers (*178*). By using extensive acrylate monomer library, linear monodisperse 18- and 20-mer acrylates were also obtained by disulfide coupling of two sequence-defined acrylate 9- and 10-mers which were initially purified by column chromatography (*179*). In addition, *in situ* generation of multiblock copolymers with ABCDE, EDCBA and EDCBABCDE sequences composed of hydrophobic, hydrophilic and fluorinated monomers was also made possible with photo-ATRP via SUMI (*172*, *180*). Further analysis with small-angle X-ray scattering (SAXS) revealed that certain sequences fluorinated monomers enabled well-ordered structures (*180*). As oligomers synthesized via radical polymerization are often polydisperse in nature, a novel strategy to prepare discrete oligomeric library with acrylates, styrenic, siloxanes as well as conjugated oligomers was developed using automated flash chromatography (*181*, *182*). This strategy allowed for preparation of discrete oligomers with distributions close to unity which provided an opportunity to study self-assembly of triplex helix stereocomplex of PMMA oligomers (*183*) and also dispersity effects on the self-assembly of oligomer composed of dimethylsiloxane-block-methyl methacrylate (*184*).

Postpolymerization Modification

Postpolymerization modification has advanced remarkably in recent decades, allowing polymer chemists to employ organic chemistry for generation of complex functional materials. Postpolymerization functionalization can be an effective technique in generating a library of functional polymer from a single parent precursor, and therefore, ensuring polymers with identical degree of polymerization, stereochemistry, and molecular weight distributions. In addition, postpolymerization functionalization also allows the attachment of functional pendant groups to polymer backbones, especially if these functional groups are too reactive to be incorporated in the initial polymer (*185*). Excellent reviews provide comprehensive coverage of past and current postpolymerization techniques (*70*, *185*, *186*). Several postpolymerization methods can serve as examples of recent progress in this field. For instance, organocatalytic transesterification with 1,5,7-triazabicyclo[4.4.0]dec-5-ene provides a new route towards site-selective acyl substitution on unhindered esters (*187*). Polyacrylates can undergo acyl substitutions with nucleophilic alcohols and amines to provide novel functional materials. In addition, a reaction of an alkyl iodide (R-I) with azide anion (N_3^-) to reversibly generate the alkyl radical was also explored to yield well defined polymers (polymer-I) through iodine mediated polymerization (Scheme 5) (*188*). This reaction was solvent selective where alkyl iodide and azide

anion generated alkyl radical in nonpolar solvent while polar solvent generated polymer terminated with an azide group. This unique solvent dependent property of the polymerization was utilized to generate initial polymer terminated with iodide in nonpolar solvent using N_3^- catalyst. Upon addition of polar solvent, azide-functionalized polymer was generated. This approach was then extended to postmodify iodide functionalized polymer brushes with azide functionality with control over the coverage of this functionality.

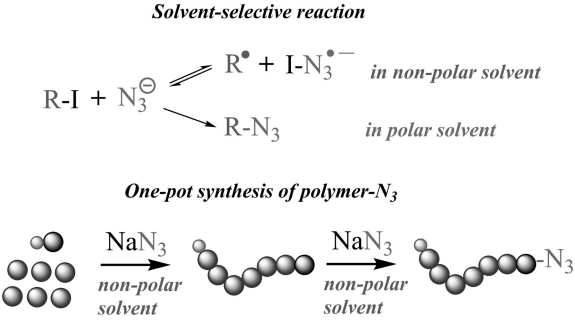

Scheme 5. Solvent selective iodine mediated polymerization with alkyl iodide and azide anion generating alkyl radical in nonpolar solvent while polar solvent led to polymer terminated with an azide group. Adapted with permission from ref. (188). Copyright 2017, American Chemical Society.

Polymeric Nanoparticles, Branched Architectures, and Gels

Novel chemistries have also been introduced for synthesis of polymeric nanoparticle through polymerization induced self-assembly (PISA) as well as branched architecture with both ATRP and RAFT methods. As several excellent reviews and articles have been published on PISA, this area will not be covered in this section and interested readers are referred to them (*136*, *189–195*). In terms of novel branched material synthesis, several synthetic discoveries have been made via photo and thermal means. Exploration of porphyrins for photoRAFT polymerization led to the discovery of pheophorbide *a* (PheoA) photocatalyst that selectively activated dithiobenzoate and ZnTPP that selectively activated trithiocarbonate. This discovery was used to synthesize one-pot, two-step graft copolymer of (PMMA-*r*-BTPEMA)-*g*-PMMA by manipulation of wavelengths to activate different photocatalysts at different instances (*196*, *197*). In addition, limitation of additive manufacturing, where terminated chains unable to further chain extend to introduce new functionalities, was also solved with ATRP and RAFT. A novel approach called Photo-Redox Catalyzed Growth (PRCG) where a "living" 3D parent gel was first grown via strain promoted alkyne-azide cycloaddition (SPAAC) of 4-arm polyethylene glycol (PEG) star polymer with dibenzocyclooctyne (Tetra-DBCO-PEG) and a bis-azide TTC (bis-N_3-TTC) in the presence of monomer, PTH photocatalyst, and/or

crosslinker to form a network of homogenous polymers was introduced (*198*). Photoactivation of PTH led to the expansion of the polymer network with the generation of daughter network that can be chemically similar or differentiated from the parent gel. Furthermore, the concept of Structurally Tailored and Engineered Macromolecular gel (STEM gel) was introduced to overcome the limitations of free radical additive manufacturing (*199*). The parent network was initially designed via free radical copolymerization of different monomers, a crosslinker, and a photo-active dormant initiator/monomer (inimer) based on the radical photoinitiator 2-hydroxy-4'-(2-hydroxyethoxy)-2-methylpropiophenone (Irgacure 2959) with latent initiating sites for post-polymerization of secondary network. The secondary network was then generated through infiltration of monomers followed by activation under UV light resulting in materials spatially differentiated mechanical properties (*200*). Reversible covalent chemistry was also introduced to alter the topology of polymers, which often is an inalterable post-synthetic feature (Scheme 6) (*201*). This approach, termed macromolecular metamorphosis, allows for linear amphiphilic block copolymer or hyperbranched polymers synthesized through ATRP to undergo metamorphosis to generate comb, star, hydrophobic and block copolymer architectures. In addition, applying this chemistry to macroscopic gel led to transition from densely covalent crosslinked network to a network with large distances between covalent crosslinks. The core chemistry of this approach relied on Diels-Alder [4+2] cycloaddition between a diene and a dienophile where furan-maleimide and anthracene-maleimide conjugations were explored. Most furan-maleimide functionalities are conjugated at ambient-to-moderate temperatures, whereas the reverse reaction is favored at higher temperatures. The conjugation between anthracene-maleimide is often near-quantitative at elevated temperatures. Further DFT calculations also revealed that the activation energy for furan-maleimide cycloreversion reaction was comparable to the anthracene-maleimide cycloaddition. Consequently, this allowed for anthracene-maleimide cycloaddition upon cleavage of furan-maleimide adduct, and therefore, afforded metamorphosis of architecture.

Advances in Organic-Inorganic Hybrid Materials

Polymer brushes consist of polymer chains covalently bonded to a substrate (inorganic surface or a polymer backbone). Current RDRP techniques enable the growth of polymer brush architectures with uniform molecular weight and narrow distributions from initiator sites bound to surfaces, and therefore, enabling control over brush density and chain conformation (*202*). Polymer brushes find applications in areas such as drug delivery (*203*) and antifouling surfaces (*204*). Two important strategies are often employed for grafting of polymers from surfaces which include "grafting to" (attachment of polymer chains to a substrate), and "grafting from" (growing polymer chains from initiator sites on a substrate). Several reviews summarized the recent advancements in this field (*205–211*). A recent work employed a universal tetherable initiator structurally analogous to fatty acid chains, 12-(2-bromoisobutyramido)dodecanoic acid (BiBADA), which was used for surface initiated ATRP (SI-ATRP) polymerization from metal oxide

nanoparticles (Scheme 7) (*212*). Nanoparticles such as sub-10 nm Fe_3O_4 as well as aluminum foil were modified with BiBADA initiator to grow PMMA or PBA brushes.

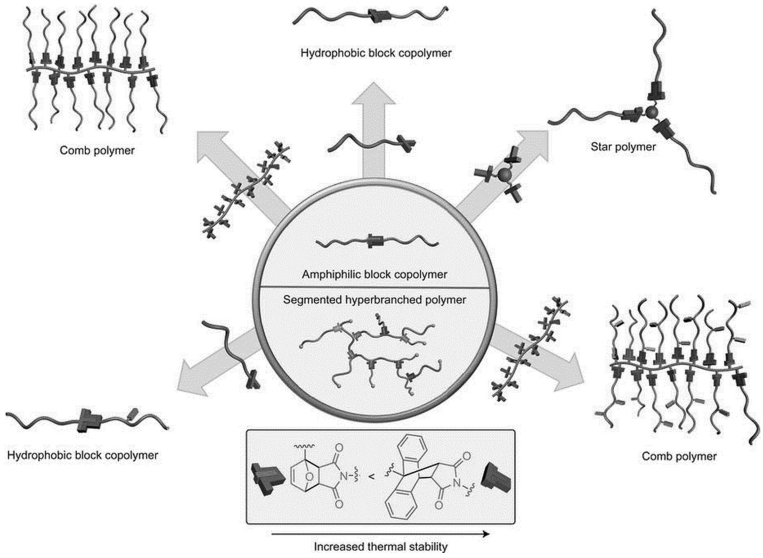

Scheme 6. Altering the topology of polymers through macromolecular metamorphosis. Reproduced with permission from ref. (201). Copyright 2017, Nature Publisher Ltd.

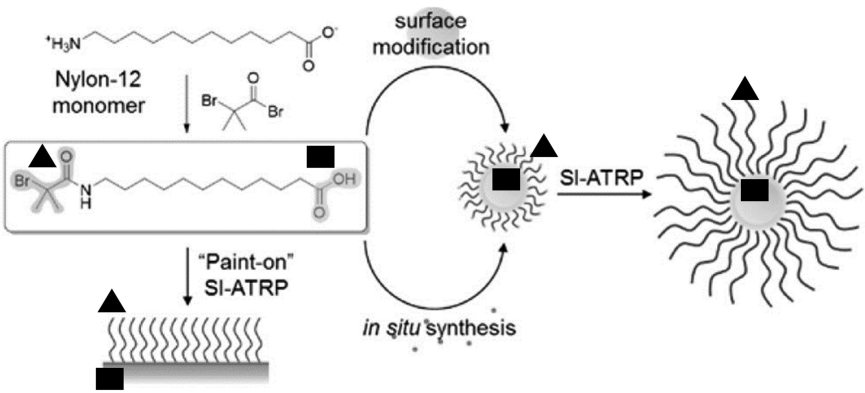

Scheme 7. Universal tetherable initiator structurally analogous to fatty acid chains, 12-(2-bromoisobutyramido)dodecanoic acid (BiBADA) for surface initiated ATRP (SI-ATRP) polymerization from metal oxide nanoparticles. Reproduced with permission from ref. (212). Copyright 2017, American Chemical Society.

In addition, tethering of polymer chains with bimodal molecular weight distributions has enabled the screening of particle core interactions that often result in complexation and also the sparse high molecular weight chains provide entanglement and enhanced mechanical properties (*213*, *214*). SI-ATRP is a versatile technique to generate monomodal grafting of PMMA using photocatalysts such as PTH on silica surfaces (*215*). Moreover, SI-ATRP was also used to promote bimodal graft modification where polystyrene-tethered silica with a small fraction of high molecular weight chains increased mechanical strength of particle films compared to densely tethered particle systems (*216*). Silica particles tethered with polymers, composed of MMA, St and copolymers of St and acrylonitrile, were used to study upper or lower critical solution temperature (UCST/LCST)-type phase behavior in binary particle mixtures (*217*). Upon heating and cooling, the polymer-tethered particle blends organized into microdomain structures depending on the LCST or UCST of the particles. The particle microdomains can also be tuned by varying the polymer composition and thermal process conditions. In addition, the properties of polystyrene modified silica nanoparticles in terms of deformation characteristics and processability of particle assembly structures were studied by factoring in the particle size and degree of polymerization of surface tethered chains (*218*). An increase in fracture toughness was observed when the degree of polymerization exceeded a threshold (transition of tethered chains from stretched-to-relaxed conformation), a value that increases with particle size. In addition, increase in particle size resulted in reduced toughness due to decrease in entanglement density with increasing space in particle array structures.

A novel aqueous based approach for scalable synthesis of nitrogen-doped porous carbons with high specific surface area and nitrogen content was applied to both inorganic and all-organic templating (i.e. silica nanoparticles, nanocellulose fillers or filter paper) (Scheme 8) (*219*). Zinc chloride ($ZnCl_2$) was an important component of the system as it solubilized polyacrylonitrile (PAN) and also acted as volatile porogen during PAN pyrolysis. It also aided to form mesoporous structures, and therefore, increased the specific surface area. The generated materials portrayed excellent catalytic activity in oxygen reduction reaction via the four-electron mechanism. Moreover, a novel approach was also explored to synthesize anisotropic titania hybrid nanocomposites where linear and four-arm molecular bottlebrushes composed of poly(acrylic acid)-block-polystyrene (PAA-b-PSt) side chains were synthesized through "grafting-from" approach and used as templates to prepare hybrid nanocomposites (*220*). This approach allowed for structural features such as anisotropy and morphologies of the branches to be transferred into hybrid nanocomposites. Despite having different PSt content blocks, the length of PAA segments dictated the diameter of the worm-like micelle that formed with titania nanoparticle. The boundary of the titania nanoparticle was defined by the interface between the two blocks.

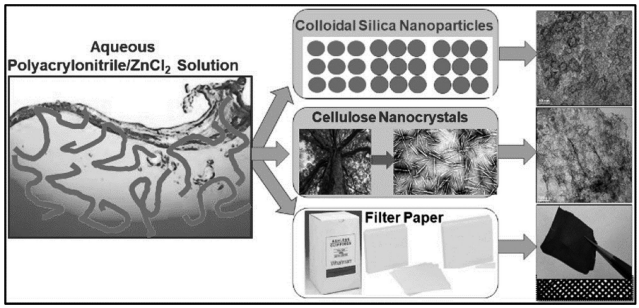

Scheme 8. Synthesis of novel nitrogen-doped porous carbons with high specific surface area and nitrogen content for inorganic and all-organic templating. Reproduced with permission from ref. (219). Copyright 2017, American Chemical Society.

Polydopamine layer which deposits on virtually any surface and substrate was developed as a photoinitiating layer for free radical polymerization for a variety of monomers including styrene, acrylates, acrylamides and methacrylates (*221*). Mussel inspired chemistry was also utilized for surface modification of carbon nanotubes (CNTs) through chain transfer free radical polymerization using cysteamine hydrochloride as chain transfer agent and methacryloyloxyethyl trimethylammonium chloride (MTC) as the monomer (*222*). The surface modification with PMTC led to better dispersability of CNTs in aqueous and organic solutions. This approach required no photoinitiator or photocatalyst and enabled spatial control for patterning and generating gradient polymer brushes by manipulating area of irradiation. This polydopamine was also employed for surface modification of ordered mesoporous carbons (OMCs) which increased the hydrophilicity and uranium binding by OMCs (*223*). The introduction of α-bromoisobutyryl bromide (BiBB) initiator to the PDA-coated OMCs enabled the growth of polymer brushes via ARGET-ATRP.

Electrochemical ATRP (eATRP) via bipolar electrochemical method was employed for the fabrication of both gradient (*224*) and patterned polymer brushes (*52*). A potential gradient generated from a bipolar electrode led to the formation of concentration gradient of copper(I) from one electron reduction to generate copper(II). Consequently, this resulted in the gradient growth of PNIPAM, PMMA, poly(2-hydroxy ethyl methacrylate) (PHEMA), and poly(sodium methacrylate) (PSM) brushes from substrate surface close to bipolar electrode. Manipulation of electrolytic conditions enabled generation of 3D gradient shapes, including circular pattern, with control over thickness, steepness, and modified area.

Advances in Bioconjugation

Several reviews highlighted protein-polymer, DNA-polymer bioconjugation, and glycopolymer conjugates (*69*, *134*, *225–229*). In the field of protein-polymer conjugates, a viable strategy to enable delivery of oral biomacromolecular therapeutics was studied (Scheme 9) (*230*).

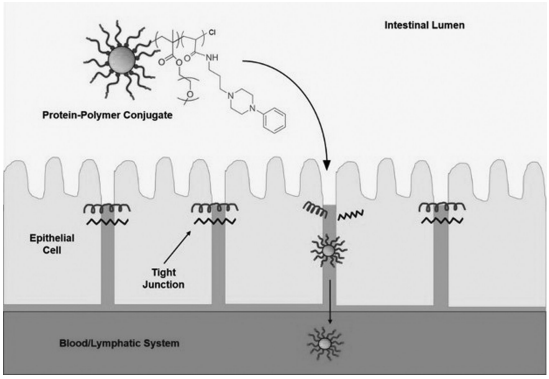

Scheme 9. Reducing toxicity of chemical permeation enhancer 1-phenylpiperazine by colocalization of the enhancer with protein bovine serum albumin (BSA) using ATRP. Reproduced with permission from ref. (230). Copyright 2017, Elsevier.

As current protein-polymer conjugates are limited by size for absorption across intestinal epithelium, toxic chemical permeation enhancers need to be used to improve macromolecular transport. However, as the toxicity of the enhancers, such as 1-phenylpiperazine, comes from non-specific permeation in the intestine, it can be reduced by colocalization of the enhancer with the protein drug. Thus, phenylpiperazine acrylamide monomer was synthesized and chain extended with ATRP from protein bovine serum albumin (BSA). An overall increase in BSA permeability was observed at non-cytotoxic doses of phenylpiperazine.

Protein-Polymer Conjugation

Physicochemical interactions between polymer and protein and the impact of this interaction on the overall stability and activity of the protein are poorly understood. To fill this gap in the literature, polymer physicochemical properties on the properties and stability of the chymotrypsin–polymer conjugates and their degree of binding to intestinal mucin, bioactivity, and stability in stomach acid were investigated by synthesizing cationic, zwitterionic, uncharged, and anionic polymers using "grafting-from" ATRP (*231*). Enzyme activity increased at pH 6-8 with cationic polymers while activity was reduced for uncharged and anionic polymers. No change in chymotrypsin activity was seen for zwitterionic polymers. Appropriate modification of chymotrypsin retained it activity also in organic solvents (*232*). Cationic polymers also led to decreased structural unfolding at lower pH unlike unfolding of proteins conjugated with uncharged

and anionic polymers which were quick. The degree to which the polymers interacted with protein surface determined whether the protein was stabilized or inactivated due to removal of water (*233*).

Almost all Food and Drug Administration (FDA)-approved protein conjugates are covalently linked to poly(ethylene glycol) (PEG) (*234*). PEGylation of drugs or proteins ensures a longer half-lifetime in the bloodstream, enabling less frequent dosing for patients with branched PEG polymers conferring additional stability and advantageous properties compared to linear PEGs (*235*). Nevertheless, PEG was shown to cause hypersensitivity and immunological responses, accumulation in tissues and rapid blood clearance upon repeated exposure (*234*). The non-biodegradable nature of PEG leads to vacuoles in organs such as the liver, kidney, and spleen with potential degradation under light, heat and mechanical stress to toxic side products (*234*). Consequently, the potential drawbacks of PEG led to the development of alternatives. For instance, a recent work looked into the synthesis of a novel sulfoxide-based water soluble polymer poly(2-(methylsulfinyl)ethyl acrylate) (PMSEA) using ARGET-ATRP (*236*). Well defined linear polymers and star polymers via "arm-first" approach or a "core-first" approach using a biodegradable β-cyclodextrin core were grown. Interestingly, the linear and star polymer of PMSEA showed low toxicity to human embryonic kidney cells (HEK 293) to concentrations up to 3 mg/mL. The facile synthesis, water solubility, and low toxicity of PMSEA provide an opportunity as a potential replacement for polymers such as PEG, POEGMA, and polyoxazolines.

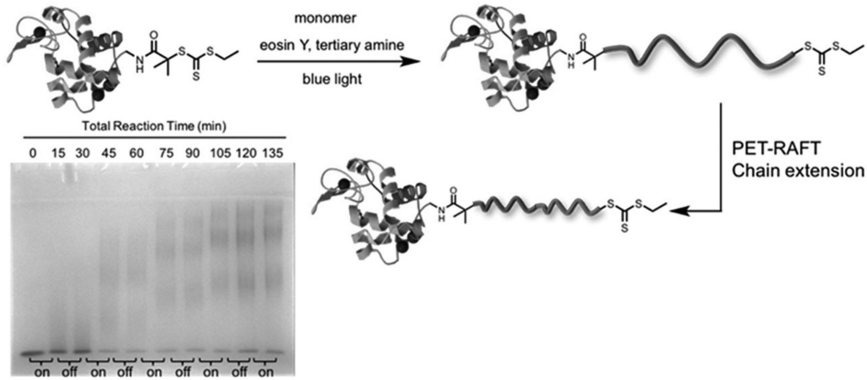

Scheme 10. Novel strategy for grafting polymer from protein surfaces using metal-free RAFT polymerization. Reprinted with permission from ref. (237). Copyright 2017, American Chemical Society.

In addition to novel monomer synthesis, innovations in the synthetic methods to generate protein-polymer conjugates have also been pursued. For instance, PET-RAFT polymerization catalyzed by metal-free EY and tertiary amine was employed to graft polymers from protein under visible light irradiation (Scheme

10). This approach enabled the generation of well-defined protein-polymer conjugates as well as temporal control on the overall synthesis (*237*). In addition, iron porphyrin derived from the active center of proteins such as horse radish peroxidase and hemoglobin were successfully implemented for ATRP of MAA which led to PMAA with molecular weights over 20 000 and low dispersities (*238*). This discovery opens up opportunities to use biocompatible naturally derived enzymatic catalysts for polymer-protein conjugation.

DNA-Polymer Conjugations

In terms of advancement in DNA-polymer conjugates, automated synthesis of polymers with commercially available DNA/RNA synthesizer was used for synthesis of homopolymers, block copolymers and DNA-polymer hybrids (*239*). Photo-ATRP was employed to perform oxygen tolerant polymerizations of acrylates and methacrylates. Next, grafting of polymers, such as hydrophilic (POEGA) and hydrophobic (PMA), from DNA strand to realize DNA-polymer hybrids was carried out. DNA oligonucleotide (SeqAA, 5'- ATC TGA GAC TCA CTG-3') was employed with a Cy3 dye conjugated to the 3'-end, as an indicator of DNA integrity, and α-bromoisobutyrate (iBBr) initiator conjugated to 5'-end of the DNA through phosphoramidite chemistry. Grafting of polymer chains was then carried out with photo-ATRP.

In addition, as fluorescence detection of DNA often requires a strong signal output at native expression levels, an increase in fluorescent labels are required. However, this strategy often results in the crowding-induced self-quenching of chromophores. This limitation was overcome by using DNA-polymer macromolecular scaffold (Scheme 11) (*240*).

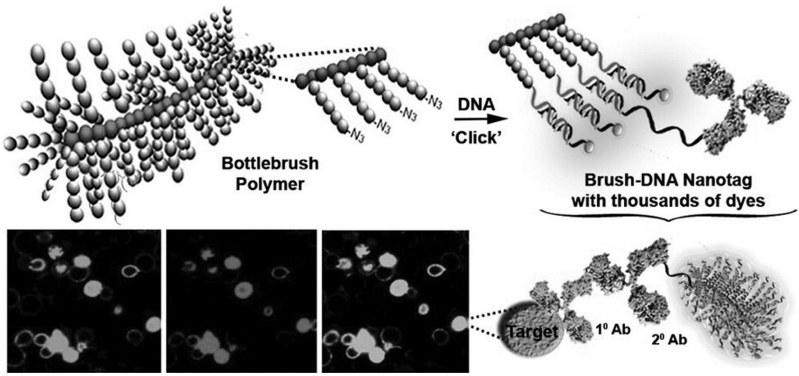

Scheme 11. Generation of bottlebrush polymers that extend hundreds of duplex DNA strands that can accommodate hundreds of covalently attached and/or thousands of noncovalently intercalated fluorescent dyes. Reproduced with permission from ref. (240). Published under the ACS AuthorChoice license. Copyright 2015, American Chemical Society.

A bottlebrush polymer (BBP) consisting of poly[2-(2-bromoisobutyryloxy)ethyl methacrylate] (PBiBEM) macroinitiator with a degree of polymerization of 400 was used as the backbone. Approximately 200 of the bromoisobutyrate side chains were initiated with 2-(2-(2-methoxyethoxy)-ethoxy)ethyl methacrylate monomeric units. The bromine group of the side chains were then modified into azide functionality to enable Cu(I) promoted azide-alkyne cycloaddition reaction DNA. The polymer-DNA scaffold provided a dense scaffold for intercalation of fluorescent dyes without dissociation, avoiding nonspecific fluorescence and the need for covalent attachment of dyes. The DNA bristles also allow for attachment of different terminal acceptor dyes at the end of DNA strands. DNA hybridization was then used to attach a secondary antibody for targeting, and therefore, generating a probe that was at least 10 times brighter than commercially available quantum dots or Alexa fluor-tagged IgG antibodies under identical conditions. This technology provides an opportunity for selective targeting of intracellular compartments based on attached antibody and can be further developed into *in vitro* detection assays.

Glycopolymer Conjugates

Glycopolymer conjugates, especially polymers modified with trehalose, have improved external stability and the *in vivo* plasma half-life of a therapeutic protein (*241*). In a model study with insulin, the addition of glycopolymer as an excipient or covalent conjugation prevented thermal or agitation-induced aggregation of insulin (*242*). Similar to PEG, insulin-trehalose glycopolymer conjugate prolonged plasma circulation life time in mice and maintained bioactivity at high temperature while causing no toxicity to mice at a loading of at least 1.6 mg/kg dosage. Systematic investigation on the effect of the point of linkage of trehalose to a polymer backbone was also carried out to determine whether the differences between trehalose regioisomers affected protein stabilization (*243*). Four trehalose regioisomers containing a vinylbenzyl ether moiety at either the 2-O, 3-O, 4-O, or 6-O position were synthesized and characterized. Insulin was used as the model protein to determine the ability of regioisomers of trehalose to prevent agitation-induced aggregation. This investigation revealed that there were no significant differences in terms of stabilization for the different regioisomers. Consequently, it was proposed that the clam shell conformation, bending of the anomeric position of trehalose disaccharide leading to the two glucose ring coming into close proximity, taken up the trehalose may be more important than the regiochemistry of the vinyl benzyl ether. Interestingly, a trehalose block copolycation consisting of 6-methacrylamido-6-deoxy trehalose-co-N(2-aminoethyl) methacrylamide (pMAT-b-AEMA) was an effective polyplex with short interfering RNA (siRNA) (*244*) for gene knockdown in cultured glioblastoma (U87), and pT2/CaL plasmid DNA (pDNA) (*245*) for gene delivery in U87 and human liver carcinoma (HepG2) cell lines. In both cases high stability and minimum toxicity were reported for the polyplexes.

Grafting Polymer from Living Cells

A recent development in the field of bioconjugation is direct polymer grafting from surface of living cells (*246*). The first example of direct polymer grafting from living cells was carried out with yeast cells with surface-initiated ARGET-ATRP (*247*). In this approach, a dopamine-based ATRP initiator was synthesized to enable uniform polydopamine coating on cell surfaces. The radical scavenging properties of polydopamine protected the yeast cells from radical attack. ARGET-ATRP was then employed with ascorbic acid as reducing agent to graft SM polymer from the surface of yeast cells primed with ATRP initiator. The polymer grafted yeast cells showed high cell viability (~82 %) with uniform polymer grafting proved through agglutination assay and cell-division studies. Baker's yeast (*saccharomyces cerevisiae*) was also modified by coupling dibenzocyclooctyl (DBCO)-based activated ester with cell surface amino groups followed by performing a strain-promoted cycloaddition reaction with an azide functionalized trithiocarbonate. As the cycloaddition did not affect cell viability, copolymerization of PEG and ω-azido PEG acrylamide was carried out with EY under blue light irradiation. Fluorescent measurements carried out upon conjugation of Alexa Fluor 647 DIBO showed presence of polymer at the periphery of cell surface with no disruption to the cell metabolism and proliferation. Surface modification of live mammalian cells was carried out by insertion of a lipid mimic RAFT agent instead of direct attachment to cell surface to improve cell viability. In addition to cell surface modification with RAFT agents, a simple and facile "grafting to" of functional moieties by thiol-maleimide conjugation after mild reduction of disulfides in cell surface proteins with tris(2-carboxyethyl)phosphine was demonstrated (Scheme 12) (*248*). This approach was successfully implemented in a variety of cells including HeLa, Jurkat T, C2C12, Neuro-2a (N2A), human mesenchymal stem cells (hMSC), and human induced neural stem cells (hiNSC) without any disruption to cell functions. Through this approach coating of fluorescent dyes, biopolymer (chondroitin sulfate and PEG), and fluorescent labelled mesoporous silica nanoparticle (MSN) were successfully coated onto HeLa cell surfaces. HeLa cells surface with MSN loaded with rhodamine and coated with PEG showed enhanced luminescence activity when subcutaneously injected to mice with normal immunity. This approach can be readily translated for use in cells such as cancer immunotherapy and hematopoietic stem cell transplantation. In addition to cell surface modifications, yeast cells also accommodated the growth of polymeric nanoparticles within their extracellular matrix (*249*). Free radical polymerization of styrene within yeast cells generated pomegranate-like polystyrene nanoparticles which were selectively taken up by macrophage cells. The yeast cell filled with polystyrene nanoparticle acted as a Trojan particle capable of releasing its cargo in a circumstance. The ability to grow polymeric nanoparticles within yeast cells helped to overcome the permeability restriction for diffusion of nanoparticles into the yeast cells, and therefore, provided a novel avenue for nanoparticle delivery.

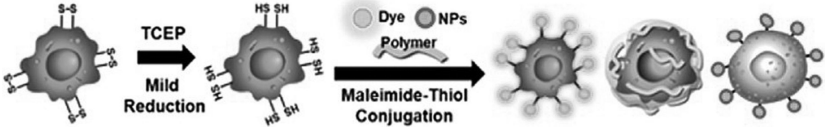

Scheme 12. Living cell surface grafting via thiol-maleimide conjugation after mild reduction of disulfides on cell surface proteins. Reproduced with permission from ref. (248). Copyright 2018, American Chemical Society.

Other Advancements

In addition to the aforementioned progress in RDRP, this section will highlight emerging methods that further improve current polymer synthesis as well as ensure feasible scale up. For instance, miniemulsion polymerization with eATRP hydrophilic complex, $Br{-}Cu^{II}TPMA^{+}$, has led to a paradigm shift as the ion pair ($Br{-}Cu^{II}TPMA^{+}/SDS^{-}$) formed with anionic surfactant, sodium dodecyl sulfate (SDS), enabled the hydrophilic complex to move into the hydrophobic PBA micelles and particles. The ion pairs are primarily situated at the surface of monomer droplets (95% of the catalyst bound to monomer/water interface), but they are able to migrate inside (1% of the catalyst) the droplets to enable ATRP polymerization (*250*). This concept was then expanded to miniemulsion via ARGET-ATRP with ascorbic acid reducing agent to enable polymerization of BA and BMA using the same catalytic system (*251*). The use of ARGET ATRP enabled miniemulsion polymerization with copper loading as low as 50 ppm and leaving behind 300 ppb in the precipitated polymer. As the polymerization portrayed excellent living characteristics, this approach was expanded for preparation of polymers with complex architectures such as block copolymers, star polymers, and molecular brushes. In terms of scale up of polymer synthesis via photopolymerization, continuous flow reactors with efficient mass- and heat-transfer and uniform irradiation for production of well-defined polymers for RAFT (*197*, *252*, *253*) and ATRP (*254*) were designed. Another important aspect of rapid scale up is the ability to quench oxygen molecules before and during the course of polymerization to reduce premature termination of radicals (*255*). This was achieved by rapidly converting inert triplet oxygen molecule to singlet oxygen which then react with singlet oxygen quenchers via PET-RAFT (*256–258*). In addition, enzyme mediated oxygen quenching pathways were introduced for ATRP and RAFT through the use of glucose oxidase which converted oxygen into hydrogen peroxide by using glucose as a substrate (*259*, *260*).

Conclusions

Recent achievements in mechanistic understandings, especially CRT in ATRP, SARA-ATRP as well as ligand design was highlighted in this review. In order to mimic biological complexity of nature in terms of macromolecular synthesis, exploration of novel initiation mechanisms for different RDRP

techniques was discussed. These novel mechanisms allowed for spatial, temporal, sequence and stereochemical control over polymer synthesis, and therefore, led to to new complex materials. The advancements in material synthesis in terms of novel architectures, polymer brushes, bioconjugates as well as the general synthetic steps in making them were highlighted.

Abbreviations

AA	acrylic acid
AIBN	azobis(isobutyronitrile)
ATRP	atom transfer radical polymerization
BA	n-butyl acrylate
$BaTiO_3$	barium titanate
BBP	bottle brush polymer
BiBADA	12-(2-bromoisobutyramido)dodecanoic acid
BiBB	α-bromoisobutyryl bromide
BiBEM	2-(2-bromoisobutyryloxy)ethyl methacrylate
BMA	*n*-butyl methacrylate
BSA	bovine serum albumin
BzMA	benzyl methacrylate
CCTP	catalytic chain transfer polymerization
CNT	carbon nanotube
CPI	2-cyanopropyl iodide
CRT	catalytic radical termination
$Cu(phen)_2^+$	bis(1,10-phenanthroline)copper(I)
DEA	*N*,*N*-diethylacrylamide
DMA	*N,N*-dimethylacrylamide
DMAc	dimethylacetamide
DMAEMA	2-(dimethylamino)ethyl methacrylate
DMF	dimethylformamide
DMSO	dimethylsulfoxide
EB	erythrosine B
EBiB	ethyl α-bromoisobutyrate
EBPA	ethyl α-bromophenylacetate
EMA	ethyl methacrylate
ESI-MS	electrospray-ionization mass spectrometry
EY	Eosin Y
fac-$Ir(ppy)_3$	Tris[2-phenylpyridinato-C^2,*N*]iridium(III)
FMA	furfuryl methacrylate
GA	glycidyl acrylate
GMA	glycidyl methacrylate
Gox	glucose oxidase
HEMA	(2-hydroxy ethyl methacrylate
iBBr	α-bromoisobutyrate
IMP	iodine mediated polymerization
Irgacure 2959	2-hydroxy-4′-(2-hydroxyethoxy)-2-methylpropiophenone

Matyjaszewski et al.; Reversible Deactivation Radical Polymerization: Mechanisms and Synthetic Methodologies
ACS Symposium Series; American Chemical Society: Washington, DC, 2018.

ISET	inner sphere electron transfer
k_a	activation rate coefficient
MA	methyl acrylate
MAA	methacrylic acid
MBrP	methyl 2-bromopropionate
Me_6TREN	tris[2-(dimethylamino)ethyl]amine
MMA	methyl methacrylate
MSEA	2-(methylsulfinyl)ethyl acrylate
MSN	mesoporous silica nanoparticle
NAM	4-acryloylmorpholine
NIPAM	*N*-isopropylacrylamide
OEGMA	oligo(ethylene glycol) methyl ether methacrylate
OMC	ordered mesoporous carbon
OMRP	organometallic-mediated radical polymerization
P2Ox	pyranose oxidase
PEG	poly(ethylene glycol)
Photo-RCMP	photoinduced reversible complexation mediated polymerization
PISA	polymerization induced self-assembly
PLP	pulsed-laser polymerization
PMDETA	*N*,*N*,*N*′,*N*″,*N*″-pentamethyldiethylenetriamine
PRGC	Photo-Redox Catalyzed Growth
PTH	10-phenylphenothiazine
RAFT	reversible addition-fragmentation chain transfer polymerization
RDRP	reversible-deactivation radical polymerization
SA	solketal acrylate
SEC	size exclusion chromatography
SI-ATRP	surface initiated ATRP
SM	sodium methacrylate
St	styrene
STEM	Structurally Tailored and Engineered Macromolecular
TBA	tributylamine
tBA	tert-butyl acrylate
TERP	tellurium mediated polymerization
TMSEMA	trimethylsilyloxyethyl methacrylate
TPMA	tris(2-pyridylmethyl)amine
TPMA^{*3}	tris-(3,5-dimethyl-4-methoxy-2-pyridylmethyl)amine
TPMA^{NMe2}	tris[(4-dimethylaminiopyridyl)methyl]amine
UHMW	ultra-high molecular weights
V601	dimethyl 2,2′-azobis(isobutyrate)

Acknowledgments

The support from the NSF (CHE-1707490 and DMR-1501324), DoE (9ER45998) and NIH (R01 DE0208843) is gratefully acknowledged. The authors acknowledge Thomas Ribelli and Dr. Marco Fantin for their contributions in designing the schemes.

References

1. *Controlled Radical Polymerization: Materials*; Matyjaszewski, K., Sumerlin, B. S., Tsarevsky, N. V., Chiefari, J., Eds.; ACS Symposium Series 1188; American Chemical Society: Washington, DC, 2015; pp 1−339.
2. *Controlled Radical Polymerization: Mechanisms*; Matyjaszewski, K., Sumerlin, B. S., Tsarevsky, N. V., Chiefari, J., Eds.; ACS Symposium Series 1187; American Chemical Society: Washington, DC, 2015; pp 1−309.
3. Perrier, S. *Macromolecules* **2017**, *50*, 7433–7447.
4. Pan, X.; Tasdelen, M. A.; Laun, J.; Junkers, T.; Yagci, Y.; Matyjaszewski, K. *Prog. Polym. Sci.* **2016**, *62*, 73–125.
5. Boyer, C.; Corrigan, N. A.; Jung, K.; Nguyen, D.; Nguyen, T.-K.; Adnan, N. N. M.; Oliver, S.; Shanmugam, S.; Yeow, J. *Chem. Rev.* **2016**, *116*, 1803–1949.
6. Shanmugam, S.; Xu, J.; Boyer, C. *Macromol. Rapid Commun.* **2017**, *38*, 1700143.
7. Anastasaki, A.; Nikolaou, V.; Nurumbetov, G.; Wilson, P.; Kempe, K.; Quinn, J. F.; Davis, T. P.; Whittaker, M. R.; Haddleton, D. M. *Chem. Rev.* **2016**, *116*, 835–877.
8. Mastan, E.; Zhu, S. *Macromolecules* **2015**, *48*, 6440–6449.
9. Moad, G.; Solomon, D. H. *The chemistry of radical polymerization*; Elsevier: 2006.
10. Nakamura, Y.; Ogihara, T.; Yamago, S. *ACS Macro Lett.* **2016**, *5*, 248–252.
11. Nakamura, Y.; Yamago, S. *Macromolecules* **2015**, *48*, 6450–6456.
12. Nakamura, Y.; Lee, R.; Coote, M. L.; Yamago, S. *Macromol. Rapid Commun.* **2016**, *37*, 506–513.
13. Nakamura, Y.; Ogihara, T.; Hatano, S.; Abe, M.; Yamago, S. *Chem. Eur. J.* **2017**, *23*, 1299–1305.
14. Schuh, H.-H.; Fischer, H. *Helv. Chim. Acta* **1978**, *61*, 2463–2481.
15. Ribelli, T. G.; Rahaman, S. M. W.; Matyjaszewski, K.; Poli, R. *Chem. Eur. J.* **2017**, *23*, 13879–13882.
16. Coward, D. L.; Lake, B. R. M.; Shaver, M. P. *Organometallics* **2017**, *36*, 3322–3328.
17. Shaver, M. P.; Allan, L. E. N.; Rzepa, H. S.; Gibson, V. C. *Angew. Chem., Int. Ed.* **2006**, *45*, 1241–1244.
18. Xue, Z.; Poli, R. *J. Polym. Sci., Part A: Polym. Chem.* **2013**, *51*, 3494–3504.
19. Zerk, T. J.; Bernhardt, P. V. *Inorg. Chem.* **2017**, *56*, 5784–5792.
20. Soerensen, N.; Schroeder, H.; Buback, M. *Macromolecules* **2016**, *49*, 4732–4738.

21. Ribelli, T. G.; Augustine, K. F.; Fantin, M.; Krys, P.; Poli, R.; Matyjaszewski, K. *Macromolecules* **2017**, *50*, 7920–7929.
22. Wang, Y.; Soerensen, N.; Zhong, M.; Schroeder, H.; Buback, M.; Matyjaszewski, K. *Macromolecules* **2013**, *46*, 683–691.
23. Ribelli, T. G.; Augustine, K. F.; Fantin, M.; Krys, P.; Poli, R.; Matyjaszewski, K. *Macromolecules* **2017**, *50*, 7920–7929.
24. Pintauer, T.; Matyjaszewski, K. *Chem. Soc. Rev.* **2008**, *37*, 1087–1097.
25. Kaur, A.; Ribelli, T. G.; Schröder, K.; Matyjaszewski, K.; Pintauer, T. *Inorg. Chem.* **2015**, *54*, 1474–1486.
26. Ribelli, T. G.; Wahidur Rahaman, S. M.; Krys, P.; Matyjaszewski, K.; Poli, R. *Macromolecules* **2016**, *49*, 7749–7757.
27. Ribelli, T. G.; Fantin, M.; Daran, J.-C.; Augustine, K. F.; Poli, R.; Matyjaszewski, K. *J. Am. Chem. Soc.* **2018**, *140*, 1525–1534.
28. Matyjaszewski, K.; Tsarevsky, N. V.; Braunecker, W. A.; Dong, H.; Huang, J.; Jakubowski, W.; Kwak, Y.; Nicolay, R.; Tang, W.; Yoon, J. A. *Macromolecules* **2007**, *40*, 7795–7806.
29. Konkolewicz, D.; Wang, Y.; Krys, P.; Zhong, M.; Isse, A. A.; Gennaro, A.; Matyjaszewski, K. *Polym. Chem.* **2014**, *5*, 4396–4417.
30. Peng, C.-H.; Zhong, M.; Wang, Y.; Kwak, Y.; Zhang, Y.; Zhu, W.; Tonge, M.; Buback, J.; Park, S.; Krys, P.; Konkolewicz, D.; Gennaro, A.; Matyjaszewski, K. *Macromolecules* **2013**, *46*, 3803–3815.
31. Zhong, M.; Wang, Y.; Krys, P.; Konkolewicz, D.; Matyjaszewski, K. *Macromolecules* **2013**, *46*, 3816–3827.
32. Whitfield, R.; Anastasaki, A.; Nikolaou, V.; Jones, G. R.; Engelis, N. G.; Discekici, E. H.; Fleischmann, C.; Willenbacher, J.; Hawker, C. J.; Haddleton, D. M. *J. Am. Chem. Soc.* **2017**, *139*, 1003–1010.
33. Krys, P.; Wang, Y.; Matyjaszewski, K.; Harrisson, S. *Macromolecules* **2016**, *49*, 2977–2984.
34. Krys, P.; Ribelli, T. G.; Matyjaszewski, K.; Gennaro, A. *Macromolecules* **2016**, *49*, 2467–2476.
35. Wang, Y.; Zhong, M.; Zhu, W.; Peng, C.-H.; Zhang, Y.; Konkolewicz, D.; Bortolamei, N.; Isse, A. A.; Gennaro, A.; Matyjaszewski, K. *Macromolecules* **2013**, *46*, 3793–3802.
36. Harrisson, S.; Nicolas, J. *ACS Macro Lett.* **2014**, *3*, 643–647.
37. Harrisson, S.; Couvreur, P.; Nicolas, J. *Macromolecules* **2012**, *45*, 7388–7396.
38. Ribelli, T. G.; Krys, P.; Cong, Y.; Matyjaszewski, K. *Macromolecules* **2015**, *48*, 8428–8436.
39. Tang, W.; Kwak, Y.; Braunecker, W.; Tsarevsky, N. V.; Coote, M. L.; Matyjaszewski, K. *J. Am. Chem. Soc.* **2008**, *130*, 10702–10713.
40. Augustine, K. F.; Ribelli, T. G.; Fantin, M.; Krys, P.; Cong, Y.; Matyjaszewski, K. *J. Polym. Sci., Part A: Polym. Chem.* **2017**, *55*, 3048–3057.
41. Magenau, A. J. D.; Strandwitz, N. C.; Gennaro, A.; Matyjaszewski, K. *Science* **2011**, *332*, 81–84.
42. Bortolamei, N.; Isse, A. A.; Magenau, A. J. D.; Gennaro, A.; Matyjaszewski, K. *Angew. Chem. Int. Ed.* **2011**, *123*, 11593–11596.

43. Park, S.; Chmielarz, P.; Gennaro, A.; Matyjaszewski, K. *Angew. Chem. Int. Ed.* **2015**, *127*, 2418–2422.
44. Strover, L. T.; Malmström, J.; Stubbing, L. A.; Brimble, M. A.; Travas-Sejdic, J. *Electrochim Acta* **2016**, *188*, 57–70.
45. Guo, J.-K.; Zhou, Y.-N.; Luo, Z.-H. *Macromolecules* **2016**, *49*, 4038–4046.
46. Fantin, M.; Park, S.; Wang, Y.; Matyjaszewski, K. *Macromolecules* **2016**, *49*, 8838–8847.
47. Sun, Y.; Du, H.; Lan, Y.; Wang, W.; Liang, Y.; Feng, C.; Yang, M. *Biosens. Bioelectron.* **2016**, *77*, 894–900.
48. Guo, J.-K.; Zhou, Y.-N.; Luo, Z.-H. *AIChE J.* **2015**, *61*, 4347–4357.
49. Li, B.; Yu, B.; Huck, W. T. S.; Zhou, F.; Liu, W. *Angew. Chem., Int. Ed.* **2012**, *51*, 5092–5095.
50. Park, S.; Cho, H. Y.; Wegner, K. B.; Burdynska, J.; Magenau, A. J. D.; Paik, H.-j.; Jurga, S.; Matyjaszewski, K. *Macromolecules* **2013**, *46*, 5856–5860.
51. Magenau, A. J. D.; Bortolamei, N.; Frick, E.; Park, S.; Gennaro, A.; Matyjaszewski, K. *Macromolecules* **2013**, *46*, 4346–4353.
52. Shida, N.; Koizumi, Y.; Nishiyama, H.; Tomita, I.; Inagi, S. *Angew. Chem., Int. Ed.* **2015**, *54*, 3922–3926.
53. della Sala, F.; Chen, J. L. Y.; Ranallo, S.; Badocco, D.; Pastore, P.; Ricci, F.; Prins, L. J. *Angew. Chem., Int. Ed.* **2016**, *55*, 10737–10740.
54. Fantin, M.; Isse, A. A.; Venzo, A.; Gennaro, A.; Matyjaszewski, K. *J. Am. Chem. Soc.* **2016**, *138*, 7216–7219.
55. Chmielarz, P.; Fantin, M.; Park, S.; Isse, A. A.; Gennaro, A.; Magenau, A. J. D.; Sobkowiak, A.; Matyjaszewski, K. *Prog. Polym. Sci.* **2017**, *69*, 47–78.
56. Chen, M.; Zhong, M.; Johnson, J. A. *Chem. Rev.* **2016**, *116*, 10167–10211.
57. Corrigan, N.; Shanmugam, S.; Xu, J.; Boyer, C. *Chem. Soc. Rev.* **2016**, *45*, 6165–6212.
58. Pan, X.; Tasdelen, M. A.; Laun, J.; Junkers, T.; Yagci, Y.; Matyjaszewski, K. *Prog. Polym. Sci.* **2016**, *62*, 73–125.
59. Groote, R.; Jakobs, R. T. M.; Sijbesma, R. P. *Polym. Chem.* **2013**, *4*, 4846–4859.
60. Lenhardt, J. M.; Black Ramirez, A. L.; Lee, B.; Kouznetsova, T. B.; Craig, S. L. *Macromolecules* **2015**, *48*, 6396–6403.
61. Stauch, T.; Dreuw, A. *Chem. Rev.* **2016**, *116*, 14137–14180.
62. Li, J.; Nagamani, C.; Moore, J. S. *Acc. Chem. Res* **2015**, *48*, 2181–2190.
63. Gois, J. R.; Konkolewic, D.; Popov, A. V.; Guliashvili, T.; Matyjaszewski, K.; Serra, A. C.; Coelho, J. F. J. *Polym. Chem.* **2014**, *5*, 4617–4626.
64. Gois, J. R.; Rocha, N.; Popov, A. V.; Guliashvili, T.; Matyjaszewski, K.; Serra, A. C.; Coelho, J. F. J. *Polym. Chem.* **2014**, *5*, 3919–3928.
65. Min, K.; Gao, H.; Matyjaszewski, K. *Macromolecules* **2007**, *40*, 1789–1791.
66. Maximiano, P.; Mendonça, P. V.; Costa, J. R. C.; Haworth, N. L.; Serra, A. C.; Guliashvili, T.; Coote, M. L.; Coelho, J. F. J. *Macromolecules* **2016**, *49*, 1597–1604.
67. Leibfarth, F. A.; Mattson, K. M.; Fors, B. P.; Collins, H. A.; Hawker, C. J. *Angew. Chem., Int. Ed.* **2013**, *52*, 199–210.

68. Anastasaki, A.; Nikolaou, V.; Haddleton, D. M. *Polym. Chem.* **2016**, *7*, 1002–1026.
69. Boyer, C.; Corrigan, N. A.; Jung, K.; Nguyen, D.; Nguyen, T.-K.; Adnan, N. N. M.; Oliver, S.; Shanmugam, S.; Yeow, J. *Chem. Rev.* **2016**, *4*, 1803–1949116.
70. Ouchi, M.; Sawamoto, M. *Macromolecules* **2017**, *50*, 2603–2614.
71. Hill, M. R.; Carmean, R. N.; Sumerlin, B. S. *Macromolecules* **2015**, *48*, 5459–5469.
72. Theriot, J. C.; McCarthy, B. G.; Lim, C.-H.; Miyake, G. M. *Macromol. Rapid Commun.* **2017**, *38*, 1700040.
73. Zivic, N.; Bouzrati-Zerelli, M.; Kermagoret, A.; Dumur, F.; Fouassier, J.-P.; Gigmes, D.; Lalevée, J. *ChemCatChem* **2016**, *8*, 1617–1631.
74. Konkolewicz, D.; Schröder, K.; Buback, J.; Bernhard, S.; Matyjaszewski, K. *ACS Macro Lett.* **2012**, *1*, 1219–1223.
75. Koyama, D.; Dale, H. J. A.; Orr-Ewing, A. J. *J. Am. Chem. Soc.* **2018**, *140*, 1285–1293.
76. Mosnacek, J.; Eckstein-Andicsova, A.; Borska, K. *Polym. Chem.* **2015**, *6*, 2523–2530.
77. Borská, K.; Moravčíková, D.; Mosnáček, J. *Macromol. Rapid Commun.* **2017**, *38*, 1600639.
78. Pan, X.; Malhotra, N.; Simakova, A.; Wang, Z.; Konkolewicz, D.; Matyjaszewski, K. *J. Am. Chem. Soc.* **2015**, *137*, 15430–15433.
79. Ribelli, T. G.; Konkolewicz, D.; Bernhard, S.; Matyjaszewski, K. *J. Am. Chem. Soc.* **2014**, *136*, 13303–13312.
80. Ribelli, T. G.; Konkolewicz, D.; Pan, X.; Matyjaszewski, K. *Macromolecules* **2014**, *47*, 6316–6321.
81. Anastasaki, A.; Nikolaou, V.; Zhang, Q.; Burns, J.; Samanta, S. R.; Waldron, C.; Haddleton, A. J.; McHale, R.; Fox, D.; Percec, V.; Wilson, P.; Haddleton, D. M. *J. Am. Chem. Soc.* **2014**, *136*, 1141–1149.
82. Page, Z. A.; Bou Zerdan, R.; Gutekunst, W. R.; Anastasaki, A.; Seo, S.; McGrath, A. J.; Lunn, D. J.; Clark, P. G.; Hawker, C. J. *J. Polym. Sci., Part A: Polym. Chem.* **2016**, 801–807.
83. Jones, G. R.; Whitfield, R.; Anastasaki, A.; Haddleton, D. M. *J. Am. Chem. Soc.* **2016**, *138*, 7346–7352.
84. Anastasaki, A.; Nikolaou, V.; Simula, A.; Godfrey, J.; Li, M.; Nurumbetov, G.; Wilson, P.; Haddleton, D. M. *Macromolecules* **2014**, *47*, 3852–3859.
85. Nikolaou, V.; Anastasaki, A.; Brandford-Adams, F.; Whitfield, R.; Jones, G. R.; Nurumbetov, G.; Haddleton, D. M. *Polym. Chem.* **2016**, *7*, 191–197.
86. Anastasaki, A.; Nikolaou, V.; Nurumbetov, G.; Truong, N. P.; Pappas, G. S.; Engelis, N. G.; Quinn, J. F.; Whittaker, M. R.; Davis, T. P.; Haddleton, D. M. *Macromolecules* **2015**, *48*, 5140–5147.
87. Nikolaou, V.; Anastasaki, A.; Alsubaie, F.; Simula, A.; Fox, D. J.; Haddleton, D. M. *Poly. Chem.* **2015**, *6*, 3581–3585.
88. Frick, E.; Anastasaki, A.; Haddleton, D. M.; Barner-Kowollik, C. *J. Am. Chem. Soc.* **2015**, *137*, 6889–6896.

89. Yang, Q.; Dumur, F.; Morlet-Savary, F.; Poly, J.; Lalevée, J. *Macromolecules* **2015**, *48*, 1972–1980.
90. Yang, Q.; Balverde, S.; Dumur, F.; Lalevee, J.; Poly, J. *Poly. Chem.* **2016**, *7*, 6084–6093.
91. Fors, B. P.; Hawker, C. J. *Angew. Chem. Int. Ed.* **2012**, *51*, 8850–8853.
92. Ma, W.; Chen, H.; Ma, Y.; Zhao, C.; Yang, W. *Macromol. Chem. Phys.* **2014**, *215*, 1012–1021.
93. Chuang, Y.-M.; Ethirajan, A.; Junkers, T. *ACS Macro Lett.* **2014**, *3*, 732–737.
94. Melker, A.; Fors, B. P.; Hawker, C. J.; Poelma, J. E. *J. Polym. Sci., Part A: Polym. Chem* **2015**, *53*, 2693–2698.
95. Treat, N. J.; Fors, B. P.; Kramer, J. W.; Christianson, M.; Chiu, C.-Y.; Alaniz, J. R. d.; Hawker, C. J. *ACS Macro Lett.* **2014**, *3*, 580–584.
96. Pan, X.; Malhotra, N.; Zhang, J.; Matyjaszewski, K. *Macromolecules* **2015**, *48*, 6948–6954.
97. Telitel, S.; Dumur, F.; Campolo, D.; Poly, J.; Gigmes, D.; Pierre Fouassier, J.; Lalevée, J. *J. Polym. Sci., Part A: Polym. Chem.* **2015**, *54*, 702–713.
98. Wang, G.-X.; Lu, M.; Hou, Z.-H.; Gao, Y.; Liu, L.-C.; Wu, H. *J Macromol Sci A* **2014**, *51*, 565–571.
99. Telitel, S.; Dumur, F.; Campolo, D.; Poly, J.; Gigmes, D.; Pierre Fouassier, J.; Lalevée, J. *J. Polym. Sci. Part A: Polym. Chem.* **2016**, *54*, 702–713.
100. Wu, J.; Zhang, L.; Cheng, Z.; Zhu, X. *RSC Adv.* **2017**, *7*, 3888–3893.
101. Zhou, Y.-N.; Guo, J.-K.; Li, J.-J.; Luo, Z.-H. *Ind. Eng. Chem. Res.* **2016**, *55*, 10235–10242.
102. Zhou, M.-J.; He, F.; Wu, H.; Wang, G.-X.; Liu, L.-C.; Xu, W. *Iranian Polym. J.* **2017**, 1–7.
103. Dadashi-Silab, S.; Pan, X.; Matyjaszewski, K. *Macromolecules* **2017**, *50*, 7967–7977.
104. Pan, X.; Malhotra, N.; Dadashi-Silab, S.; Matyjaszewski, K. *Macromol. Rapid Commun.* **2016**, *1600651*.
105. Treat, N. J.; Sprafke, H.; Kramer, J. W.; Clark, P. G.; Barton, B. E.; Read de Alaniz, J.; Fors, B. P.; Hawker, C. J. *J. Am. Chem. Soc.* **2014**, *136*, 16096–16101.
106. Miyake, G. M.; Theriot, J. C. *Macromolecules* **2014**, *47*, 8255–8261.
107. Allushi, A.; Jockusch, S.; Yilmaz, G.; Yagci, Y. *Macromolecules* **2016**, *49*, 7785–7792.
108. Pan, X.; Lamson, M.; Yan, J.; Matyjaszewski, K. *ACS Macro Lett.* **2015**, *4*, 192–196.
109. Dadashi-Silab, S.; Pan, X.; Matyjaszewski, K. *Chem. Eur. J.* **2017**, 5972–5977.
110. Theriot, J. C.; Lim, C.-H.; Yang, H.; Ryan, M. D.; Musgrave, C. B.; Miyake, G. M. *Science* **2016**, *352*, 1082–1086.
111. Lim, C.-H.; Ryan, M. D.; McCarthy, B. G.; Theriot, J. C.; Sartor, S. M.; Damrauer, N. H.; Musgrave, C. B.; Miyake, G. M. *J. Am. Chem. Soc.* **2017**, *139*, 348–355.
112. Shanmugam, S.; Boyer, C. *Science* **2016**, *352*, 1053–1054.
113. Ramsey, B. L.; Pearson, R. M.; Beck, L. R.; Miyake, G. M. *Macromolecules* **2017**, *50*, 2668–2674.

114. Pearson, R. M.; Lim, C.-H.; McCarthy, B. G.; Musgrave, C. B.; Miyake, G. M. *J. Am. Chem. Soc.* **2016**, *138*, 11399–11407.
115. Jockusch, S.; Yagci, Y. *Polym. Chem.* **2016**, *7*, 6039–6043.
116. Liu, X.; Zhang, L.; Cheng, Z.; Zhu, X. *Polym. Chem.* **2016**, *7*, 689–700.
117. Kutahya, C.; Aykac, F. S.; Yilmaz, G.; Yagci, Y. *Polym. Chem.* **2016**, *7*, 6094–6098.
118. Yan, M.; Kawamata, Y.; Baran, P. S. *Chem. Rev.* **2017**, *117*, 13230–13319.
119. Fantin, M.; Lorandi, F.; Gennaro, A.; Isse, A. A.; Matyjaszewski, K. *Synthesis* **2017**, *49*, 3311–3322.
120. Lorandi, F.; Fantin, M.; Isse, A. A.; Gennaro, A. *Curr. Opin. Electrochem.* **2018**, *8*, 1–7.
121. Fantin, M.; Isse, A. A.; Venzo, A.; Gennaro, A.; Matyjaszewski, K. *J. Am. Chem. Soc.* **2016**, *138*, 7216–7219.
122. Fantin, M.; Isse, A. A.; Gennaro, A.; Matyjaszewski, K. *Macromolecules* **2015**, *48*, 6862–6875.
123. Hong, K.-S.; Xu, H.; Konishi, H.; Li, X. *J. Phys. Chem. Lett.* **2010**, *1*, 997–1002.
124. Mohapatra, H.; Kleiman, M.; Esser-Kahn, A. P. *Nat. Chem.* **2016**, *9*, 135.
125. Wang, Z.; Pan, X.; Yan, J.; Dadashi-Silab, S.; Xie, G.; Zhang, J.; Wang, Z.; Xia, H.; Matyjaszewski, K. *ACS Macro Lett.* **2017**, *6*, 546–549.
126. Wang, Z.; Pan, X.; Li, L.; Fantin, M.; Yan, J.; Wang, Z.; Wang, Z.; Xia, H.; Matyjaszewski, K. *Macromolecules* **2017**, *50*, 7940–7948.
127. Yamago, S.; Ukai, Y.; Matsumoto, A.; Nakamura, Y. *J. Am. Chem. Soc.* **2009**, *131*, 2100–2101.
128. Nakamura, Y.; Yamago, S. *Beilstein J. Org. Chem.* **2013**, *9*, 1607–1612.
129. Nakamura, Y.; Yu, M.; Ukai, Y.; Yamago, S. In *Controlled Radical Polymerization: Mechanisms*; ACS Symposium Series 1187; American Chemical Society: Washington, DC, 2015; pp 295−309.
130. Benedikt, S.; Moszner, N.; Liska, R. *Macromolecules* **2014**, *47*, 5526–5531.
131. Liu, X.; Zhang, L.; Cheng, Z.; Zhu, X. *Poly. Chem.* **2016**, *7*, 3576–3588.
132. Liu, X.-D.; Xu, Q.; Zhang, L.; Cheng, Z.-P.; Zhu, X. *Poly. Chem.* **2017**.
133. Ohtsuki, A.; Goto, A.; Kaji, H. *Macromolecules* **2013**, *46*, 96–102.
134. Zhou, T.; Zhu, Y.; Li, X.; Liu, X.; Yeung, K. W. K.; Wu, S.; Wang, X.; Cui, Z.; Yang, X.; Chu, P. K. *Prog. Mater. Sci* **2016**, *83*, 191–235.
135. Ohtsuki, A.; Lei, L.; Tanishima, M.; Goto, A.; Kaji, H. *J. Am. Chem. Soc.* **2015**, *137*, 5610–5617.
136. Derry, M. J.; Fielding, L. A.; Armes, S. P. *Prog. Polym. Sci.* **2016**, *52*, 1–18.
137. Liu, B.; Kazlauciunas, A.; Guthrie, J. T.; Perrier, S. *Macromolecules* **2005**, *38*, 2131–2136.
138. Tucker, B. S.; Getchell, S. G.; Hill, M. R.; Sumerlin, B. S. *Poly. Chem.* **2015**, *6*, 4258–4263.
139. Mayadunne, R. T. A.; Jeffery, J.; Moad, G.; Rizzardo, E. *Macromolecules* **2003**, *36*, 1505–1513.
140. Edmondson, S.; Osborne, V. L.; Huck, W. T. S. *Chem. Soc. Rev.* **2004**, *33*, 14–22.
141. Sumerlin, B. S.; Neugebauer, D.; Matyjaszewski, K. *Macromolecules* **2005**, *38*, 702–708.

142. Epps, T. H., III; O'Reilly, R. K. *Chem. Sci.* **2016**, *7*, 1674–1689.
143. Gody, G.; Maschmeyer, T.; Zetterlund, P. B.; Perrier, S. *Macromolecules* **2014**, *47*, 3451–3460.
144. Carmean, R. N.; Figg, C. A.; Becker, T. E.; Sumerlin, B. S. *Angew. Chem., Int. Ed.* **2016**, *55*, 8624–8629.
145. Gentekos, D. T.; Dupuis, L. N.; Fors, B. P. *J. Am. Chem. Soc.* **2016**, *138*, 1848–1851.
146. Corrigan, N.; Almasri, A.; Taillades, W.; Xu, J.; Boyer, C. *Macromolecules* **2017**, *50*, 8438–8448.
147. Mueller, L.; Jakubowski, W.; Matyjaszewski, K.; Pietrasik, J.; Kwiatkowski, P.; Chaladaj, W.; Jurczak, J. *Eur. Polym. J* **2011**, *47*, 730–734.
148. Huang, Z.; Chen, J.; Zhang, L.; Cheng, Z.; Zhu, X. *Polymers* **2016**, *8*, 59.
149. Rzayev, J.; Penelle, J. *Angew. Chem., Int. Ed.* **2004**, *43*, 1691–1694.
150. Truong, N. P.; Dussert, M. V.; Whittaker, M. R.; Quinn, J. F.; Davis, T. P. *Poly. Chem.* **2015**, *6*, 3865–3874.
151. Simms, R. W.; Cunningham, M. F. *Macromolecules* **2007**, *40*, 860–866.
152. Carmean, R. N.; Becker, T. E.; Sims, M. B.; Sumerlin, B. S. *Chem* **2017**, *2*, 93–101.
153. Liu, Z.; Lv, Y.; An, Z. *Angew. Chem. Int. Ed.* **2017**, *56*, 13852–13856.
154. Soeriyadi, A. H.; Boyer, C.; Nyström, F.; Zetterlund, P. B.; Whittaker, M. R. *J. Am. Chem. Soc.* **2011**, *133*, 11128–11131.
155. Gody, G.; Maschmeyer, T.; Zetterlund, P. B.; Perrier, S. *Nat. Commun.* **2013**, *4*, 2505.
156. Davis, K. A.; Matyjaszewski, K. *Macromolecules* **2001**, *34*, 2101–2107.
157. Anastasaki, A.; Nikolaou, V.; Pappas, G. S.; Zhang, Q.; Wan, C.; Wilson, P.; Davis, T. P.; Whittaker, M. R.; Haddleton, D. M. *Chem. Sci.* **2014**, *5*, 3536–3542.
158. Gody, G.; Maschmeyer, T.; Zetterlund, P. B.; Perrier, S. *Macromolecules* **2014**, *47*, 639–649.
159. Zetterlund, P. B.; Gody, G.; Perrier, S. *Macromol Theor Simul* **2014**, *23*, 331–339.
160. Gody, G.; Barbey, R.; Danial, M.; Perrier, S. *Poly. Chem.* **2015**, *6*, 1502–1511.
161. Martin, L.; Gody, G.; Perrier, S. *Poly. Chem.* **2015**, *6*, 4875–4886.
162. Engelis, N. G.; Anastasaki, A.; Nurumbetov, G.; Truong, N. P.; Nikolaou, V.; Shegiwal, A.; Whittaker, M. R.; Davis, T. P.; Haddleton, D. M. *Nat. Chem.* **2016**, *9*, 171.
163. Engelis, N. G.; Anastasaki, A.; Whitfield, R.; Jones, G. R.; Liarou, E.; Nikolaou, V.; Nurumbetov, G.; Haddleton, D. M. *Macromolecules* **2018**, *51*, 336–342.
164. Boyer, C.; Derveaux, A.; Zetterlund, P. B.; Whittaker, M. R. *Polym. Chem.* **2012**, *3*, 117–123.
165. Boyer, C.; Soeriyadi, A. H.; Zetterlund, P. B.; Whittaker, M. R. *Macromolecules* **2011**, *44*, 8028–8033.
166. Anastasaki, A.; Waldron, C.; Wilson, P.; Boyer, C.; Zetterlund, P. B.; Whittaker, M. R.; Haddleton, D. *ACS Macro Lett.* **2013**, *2*, 896–900.

167. Zhang, Q.; Collins, J.; Anastasaki, A.; Wallis, R.; Mitchell, D. A.; Becer, C. R.; Haddleton, D. M. *Angew. Chem., Int. Ed.* **2013**, *52*, 4435–4439.
168. Zhang, Q.; Anastasaki, A.; Li, G.-Z.; Haddleton, A. J.; Wilson, P.; Haddleton, D. M. *Polym. Chem.* **2014**, *5*, 3876–3883.
169. Zhang, Q.; Wilson, P.; Li, Z.; McHale, R.; Godfrey, J.; Anastasaki, A.; Waldron, C.; Haddleton, D. M. *J. Am. Chem. Soc.* **2013**, *135*, 7355–7363.
170. Alsubaie, F.; Anastasaki, A.; Wilson, P.; Haddleton, D. M. *Polym. Chem.* **2015**, *6*, 406–417.
171. Anastasaki, A.; Nikolaou, V.; Alsubaie, F.; Simula, A.; Waldron, C.; Lloyd, D. J.; Godfrey, J.; Nurumbetov, G.; Zhang, Q.; Wilson, P.; Kempe, K.; Haddleton, D. In *Controlled Radical Polymerization: Materials*; ACS Symposium Series 1188; American Chemical Society: Washington, DC, 2015; pp 29−45.
172. Vandenbergh, J.; Reekmans, G.; Adriaensens, P.; Junkers, T. *Chem. Sci.* **2015**, *6*, 5753–5761.
173. Chuang, Y.-M.; Wenn, B.; Gielen, S.; Ethirajan, A.; Junkers, T. *Polym. Chem.* **2015**, *6*, 6488–6497.
174. Wenn, B.; Junkers, T. *Macromolecules* **2016**, *49*, 6888–6895.
175. Anastasaki, A.; Nikolaou, V.; McCaul, N. W.; Simula, A.; Godfrey, J.; Waldron, C.; Wilson, P.; Kempe, K.; Haddleton, D. M. *Macromolecules* **2015**, *48*, 1404–1411.
176. Wenn, B.; Conradi, M.; Carreiras, A. D.; Haddleton, D. M.; Junkers, T. *Polym. Chem.* **2014**, *5*, 3053–3060.
177. Xu, J.; Fu, C.; Shanmugam, S.; Hawker, C. J.; Moad, G.; Boyer, C. *Angew. Chem., Int. Ed.* **2017**, 8376–8383.
178. Wang, Y.; Fantin, M.; Park, S.; Gottlieb, E.; Fu, L.; Matyjaszewski, K. *Macromolecules* **2017**, *50*, 7872–7879.
179. Haven, J. J.; De Neve, J. A.; Junkers, T. *ACS Macro Lett.* **2017**, *6*, 743–747.
180. Anastasaki, A.; Oschmann, B.; Willenbacher, J.; Melker, A.; Van Son, M. H. C.; Truong, N. P.; Schulze, M. W.; Discekici, E. H.; McGrath, A. J.; Davis, T. P.; Bates, C. M.; Hawker, C. J. *Angew. Chem., Int. Ed.* **2017**, *56*, 14483–14487.
181. Lawrence, J.; Goto, E.; Ren, J. M.; McDearmon, B.; Kim, D. S.; Ochiai, Y.; Clark, P. G.; Laitar, D.; Higashihara, T.; Hawker, C. J. *J. Am. Chem. Soc.* **2017**, *139*, 13735–13739.
182. Lawrence, J.; Lee, S.-H.; Abdilla, A.; Nothling, M. D.; Ren, J. M.; Knight, A. S.; Fleischmann, C.; Li, Y.; Abrams, A. S.; Schmidt, B. V. K. J.; Hawker, M. C.; Connal, L. A.; McGrath, A. J.; Clark, P. G.; Gutekunst, W. R.; Hawker, C. J. *J. Am. Chem. Soc.* **2016**, *138*, 6306–6310.
183. Ren, J. M.; Lawrence, J.; Knight, A. S.; Abdilla, A.; Zerdan, R. B.; Levi, A. E.; Oschmann, B.; Gutekunst, W. R.; Lee, S.-H.; Li, Y.; McGrath, A. J.; Bates, C. M.; Qiao, G. G.; Hawker, C. J. *J. Am. Chem. Soc.* **2018**, *140*, 1945–1951.
184. Oschmann, B.; Lawrence, J.; Schulze, M. W.; Ren, J. M.; Anastasaki, A.; Luo, Y.; Nothling, M. D.; Pester, C. W.; Delaney, K. T.; Connal, L. A.; McGrath, A. J.; Clark, P. G.; Bates, C. M.; Hawker, C. J. *ACS Macro Lett.* **2017**, *6*, 668–673.

185. Blasco, E.; Sims, M. B.; Goldmann, A. S.; Sumerlin, B. S.; Barner-Kowollik, C. *Macromolecules* **2017**, *50*, 5215–5252.
186. Delaittre, G.; Guimard, N. K.; Barner-Kowollik, C. *Acc. Chem. Res.* **2015**, *48*, 1296–1307.
187. Easterling, C. P.; Kubo, T.; Orr, Z.; Fanucci, G. E.; Sumerlin, B. S. *Chem. Sci.* **2017**, *8*, 7705–7709.
188. Wang, C.-G.; Goto, A. *J. Am. Chem. Soc.* **2017**, *139*, 10551–10560.
189. Rieger, J. *Macromol. Rapid Commun.* **2015**, *36*, 1458–1471.
190. Yeow, J.; Boyer, C. *Adv. Sci.* **2017**, *4*, 1700137.
191. Warren, N. J.; Armes, S. P. *J. Am. Chem. Soc.* **2014**, *136*, 10174–10185.
192. Canning, S. L.; Smith, G. N.; Armes, S. P. *Macromolecules* **2016**, *49*, 1985–2001.
193. Pei, Y.; Thurairajah, L.; Sugita, O. R.; Lowe, A. B. *Macromolecules* **2015**, *48*, 236–244.
194. Wang, G.; Schmitt, M.; Wang, Z.; Lee, B.; Pan, X.; Fu, L.; Yan, J.; Li, S.; Xie, G.; Bockstaller, M. R.; Matyjaszewski, K. *Macromolecules* **2016**, *49*, 8605–8615.
195. Kapishon, V.; Whitney, R. A.; Champagne, P.; Cunningham, M. F.; Neufeld, R. J. *Biomacromolecules* **2015**, *16*, 2040–2048.
196. Xu, J.; Shanmugam, S.; Fu, C.; Aguey-Zinsou, K.-F.; Boyer, C. *J. Am. Chem. Soc.* **2016**, *138*, 3094–3106.
197. Corrigan, N.; Rosli, D.; Jones, J. W. J.; Xu, J.; Boyer, C. *Macromolecules* **2016**, *49*, 6779–6789.
198. Chen, M.; Gu, Y.; Singh, A.; Zhong, M.; Jordan, A. M.; Biswas, S.; Korley, L. T. J.; Balazs, A. C.; Johnson, J. A. *ACS Cent. Sci.* **2017**, *3*, 124–134.
199. Beziau, A.; Fortney, A.; Fu, L.; Nishiura, C.; Wang, H.; Cuthbert, J.; Gottlieb, E.; Balazs, A. C.; Kowalewski, T.; Matyjaszewski, K. *Polymer* **2017**, *126*, 224–230.
200. Beziau, A.; de Menezes, R.; Biswas, S.; Singh, A.; Cuthbert, J.; Balazs, A.; Kowalewski, T.; Matyjaszewski, K. *Polymers* **2017**, *9*, 186.
201. Sun, H.; Kabb, C. P.; Dai, Y.; Hill, M. R.; Ghiviriga, I.; Bapat, A. P.; Sumerlin, B. S. *Nat. Chem.* **2017**, *9*, 817.
202. Chen, W.-L.; Cordero, R.; Tran, H.; Ober, C. K. *Macromolecules* **2017**, *50*, 4089–4113.
203. Zhang, Y.; Ang, C. Y.; Li, M.; Tan, S. Y.; Qu, Q.; Luo, Z.; Zhao, Y. *ACS Appl. Mater. Interfaces* **2015**, *7*, 18179–18187.
204. Xue, C.-H.; Guo, X.-J.; Ma, J.-Z.; Jia, S.-T. *ACS Appl. Mater. Interfaces* **2015**, *7*, 8251–8259.
205. Chen, W.-L.; Cordero, R.; Tran, H.; Ober, C. K. *Macromolecules* **2017**, *50*, 4089–4113.
206. Ayres, N. *Polym. Chem.* **2010**, *1*, 769–777.
207. Chen, T.; Amin, I.; Jordan, R. *Chem. Soc. Rev.* **2012**, *41*, 3280–3296.
208. Zoppe, J. O.; Ataman, N. C.; Mocny, P.; Wang, J.; Moraes, J.; Klok, H.-A. *Chem. Rev.* **2017**, *117*, 1105–1318.
209. Keating, J. J.; Imbrogno, J.; Belfort, G. *ACS Appl. Mater. Interfaces* **2016**, *8*, 28383–28399.

210. Khabibullin, A.; Mastan, E.; Matyjaszewski, K.; Zhu, S. *Adv. Polym. Sci.* **2016**, *270*, 29–76.
211. Hui, C. M.; Pietrasik, J.; Schmitt, M.; Mahoney, C.; Choi, J.; Bockstaller, M. R.; Matyjaszewski, K. *Chem. Mater.* **2014**, *26*, 745–762.
212. Yan, J.; Pan, X.; Wang, Z.; Lu, Z.; Wang, Y.; Liu, L.; Zhang, J.; Ho, C.; Bockstaller, M. R.; Matyjaszewski, K. *Chem. Mater.* **2017**, *29*, 4963–4969.
213. Kumar, S. K.; Benicewicz, B. C.; Vaia, R. A.; Winey, K. I. *Macromolecules* **2017**, *50*, 714–731.
214. Li, Y.; Tao, P.; Viswanath, A.; Benicewicz, B. C.; Schadler, L. S. *Langmuir* **2013**, *29*, 1211–1220.
215. Yan, J.; Pan, X.; Schmitt, M.; Wang, Z.; Bockstaller, M. R.; Matyjaszewski, K. *ACS Macro Lett.* **2016**, *5*, 661–665.
216. Yan, J.; Kristufek, T.; Schmitt, M.; Wang, Z.; Xie, G.; Dang, A.; Hui, C. M.; Pietrasik, J.; Bockstaller, M. R.; Matyjaszewski, K. *Macromolecules* **2015**, *48*, 8208–8218.
217. Schmitt, M.; Zhang, J.; Lee, J.; Lee, B.; Ning, X.; Zhang, R.; Karim, A.; Davis, R. F.; Matyjaszewski, K.; Bockstaller, M. R. *Sci. Adv.* **2016**, *2*, e1601484.
218. Schmitt, M.; Choi, J.; Min Hui, C.; Chen, B.; Korkmaz, E.; Yan, J.; Margel, S.; Burak Ozdoganlar, O.; Matyjaszewski, K.; Bockstaller, M. R. *Soft Matter* **2016**, *12*, 3527–3537.
219. Zhang, J.; Song, Y.; Kopeć, M.; Lee, J.; Wang, Z.; Liu, S.; Yan, J.; Yuan, R.; Kowalewski, T.; Bockstaller, M. R.; Matyjaszewski, K. *J. Am. Chem. Soc.* **2017**, *139*, 12931–12934.
220. Xie, G.; Ding, H.; Daniel, W. F. M.; Wang, Z.; Pietrasik, J.; Sheiko, S. S.; Matyjaszewski, K. *Polymer* **2016**, *98*, 481–486.
221. Sheng, W.; Li, B.; Wang, X.; Dai, B.; Yu, B.; Jia, X.; Zhou, F. *Chem. Sci.* **2015**, *6*, 2068–2073.
222. Wan, Q.; Tian, J.; Liu, M.; Zeng, G.; Huang, Q.; Wang, K.; Zhang, Q.; Deng, F.; Zhang, X.; Wei, Y. *Appl. Surf. Sci.* **2015**, *346*, 335–341.
223. Song, Y.; Ye, G.; Wu, F.; Wang, Z.; Liu, S.; Kopeć, M.; Wang, Z.; Chen, J.; Wang, J.; Matyjaszewski, K. *Chem. Mater.* **2016**, *28*, 5013–5021.
224. Li, B.; Yu, B.; Huck, W. T. S.; Liu, W.; Zhou, F. *J. Am. Chem. Soc.* **2013**, *135*, 1708–1710.
225. Averick, S.; Mehl, R. A.; Das, S. R.; Matyjaszewski, K. *J. Controlled Release* **2015**, *205*, 45–57.
226. Carmali, S.; Murata, H.; Cummings, C.; Matyjaszewski, K.; Russell, A. J. Polymer-Based Protein Engineering: Synthesis and Characterization of Armored, High Graft Density Polymer–Protein Conjugates. In *Methods in Enzymology*, first ed.; Kumar, C. V., Ed.; Academic Press: Cambridge, MA, 2017; Vol. 590, pp 347−380.
227. Lutz, J.-F.; Lehn, J.-M.; Meijer, E. W.; Matyjaszewski, K. *Nat. Rev. Mater.* **2016**, *1*, 16024.
228. Lligadas, G.; Grama, S.; Percec, V. *Biomacromolecules* **2017**, *18*, 1039–1063.

229. Tokura, Y.; Jiang, Y.; Welle, A.; Stenzel, M. H.; Krzemien, K. M.; Michaelis, J.; Berger, R.; Barner-Kowollik, C.; Wu, Y.; Weil, T. *Angew. Chem., Int. Ed.* **2016**, *55*, 5692–5697.
230. Cummings, C. S.; Fein, K.; Murata, H.; Ball, R. L.; Russell, A. J.; Whitehead, K. A. *J. Controlled Release* **2017**, *255*, 270–278.
231. Cummings, C. S.; Campbell, A. S.; Baker, S. L.; Carmali, S.; Murata, H.; Russell, A. J. *Biomacromolecules* **2017**, *18*, 576–586.
232. Cummings, C. S.; Murata, H.; Matyjaszewski, K.; Russell, A. J. *ACS Macro Lett.* **2016**, *5*, 493–497.
233. Leng, C.; Hung, H.-C.; Sun, S.; Wang, D.; Li, Y.; Jiang, S.; Chen, Z. *ACS Appl. Mater. Interfaces* **2015**, *7*, 16881–16888.
234. Pelegri-O'Day, E. M.; Lin, E.-W.; Maynard, H. D. *J. Am. Chem. Soc.* **2014**, *136*, 14323–14332.
235. Nauka, P. C.; Lee, J.; Maynard, H. D. *Polym. Chem.* **2016**, *7*, 2352–2357.
236. Li, J.; Ding, C.; Zhang, Z.; Pan, X.; Li, N.; Zhu, J.; Zhu, X. *Macromol. Rapid Commun.* **2017**, *38*, 1600482.
237. Tucker, B. S.; Coughlin, M. L.; Figg, C. A.; Sumerlin, B. S. *ACS Macro Lett.* **2017**, 452–457.
238. Fu, L.; Simakova, A.; Fantin, M.; Wang, Y.; Matyjaszewski, K. *ACS Macro Lett.* **2018**, *7*, 26–30.
239. Pan, X.; Lathwal, S.; Mack, S.; Yan, J.; Das, S. R.; Matyjaszewski, K. *Angew. Chem., Int. Ed.* **2017**, *129*, 2784–2787.
240. Fouz, M. F.; Mukumoto, K.; Averick, S.; Molinar, O.; McCartney, B. M.; Matyjaszewski, K.; Armitage, B. A.; Das, S. R. *ACS Cent. Sci.* **2015**, *1*, 431–438.
241. Boehnke, N.; Kammeyer, J. K.; Damoiseaux, R.; Maynard, H. D. *Adv. Funct. Mater.* **2018**, *28*, 1705475.
242. Liu, Y.; Lee, J.; Mansfield, K. M.; Ko, J. H.; Sallam, S.; Wesdemiotis, C.; Maynard, H. D. *Bioconjugate Chem.* **2017**, *28*, 836–845.
243. Messina, M. S.; Ko, J. H.; Yang, Z.; Strouse, M. J.; Houk, K. N.; Maynard, H. D. *Polym. Chem.* **2017**, *8*, 4781–4788.
244. Sizovs, A.; Xue, L.; Tolstyka, Z. P.; Ingle, N. P.; Wu, Y.; Cortez, M.; Reineke, T. M. *J. Am. Chem. Soc.* **2013**, *135*, 15417–15424.
245. Tolstyka, Z. P.; Phillips, H.; Cortez, M.; Wu, Y.; Ingle, N.; Bell, J. B.; Hackett, P. B.; Reineke, T. M. *ACS Biomater. Sci. Eng.* **2016**, *2*, 43–55.
246. Niu, J.; Lunn, D. J.; Pusuluri, A.; Yoo, J. I.; O'Malley, M. A.; Mitragotri, S.; Soh, H. T.; Hawker, C. J. *Nat. Chem.* **2017**, *7*, 537–545.
247. Kim, J. Y.; Lee, B. S.; Choi, J.; Kim, B. J.; Choi, J. Y.; Kang, S. M.; Yang, S. H.; Choi, I. S. *Angew. Chem., Int. Ed.* **2016**, *55*, 15306–15309.
248. Kim, H.; Shin, K.; Park, O. K.; Choi, D.; Kim, H. D.; Baik, S.; Lee, S. H.; Kwon, S.-H.; Yarema, K. J.; Hong, J.; Hyeon, T.; Hwang, N. S. *J. Am. Chem. Soc.* **2018**, *140*, 1199–1202.
249. Ma, G.; Zhao, Z.; Liu, H. *Macromolecules* **2016**, *49*, 1545–1551.
250. Fantin, M.; Chmielarz, P.; Wang, Y.; Lorandi, F.; Isse, A. A.; Gennaro, A.; Matyjaszewski, K. *Macromolecules* **2017**, *50*, 3726–3732.
251. Wang, Y.; Lorandi, F.; Fantin, M.; Chmielarz, P.; Isse, A. A.; Gennaro, A.; Matyjaszewski, K. *Macromolecules* **2017**, *50*, 8417–8425.

252. Chen, M.; Johnson, J. A. *Chem. Commun.* **2015**, *51*, 6742–6745.
253. Junkers, T.; Wenn, B. *React. Chem. Eng.* **2016**, *1*, 60–64.
254. Ramsey, B. L.; Pearson, R. M.; Beck, L. R.; Miyake, G. M. *Macromolecules* **2017**, *50*, 2668–2674.
255. Ligon, S. C.; Husár, B.; Wutzel, H.; Holman, R.; Liska, R. *Chem. Rev.* **2014**, *114*, 557–589.
256. Xu, J.; Jung, K.; Atme, A.; Shanmugam, S.; Boyer, C. *J. Am. Chem. Soc.* **2014**, *136*, 5508–5519.
257. Shanmugam, S.; Xu, J.; Boyer, C. *J. Am. Chem. Soc.* **2015**, *137*, 9174–9185.
258. Shanmugam, S.; Xu, J.; Boyer, C. *Macromolecules* **2017**, *50*, 1832–1846.
259. Enciso, A. E.; Fu, L.; Russell, A. J.; Matyjaszewski, K. *Angew. Chem., Int. Ed.* **2018**, *57*, 933–936.
260. Chapman, R.; Gormley, A. J.; Herpoldt, K.-L.; Stevens, M. M. *Macromolecules* **2014**, *47*, 8541–8547.